Article

Spatiotemporal Analysis and Prediction of Carbon Emissions from Energy Consumption in China through Nighttime Light Remote Sensing

Zhaoxu Zhang [1,2,3], Shihong Fu [1], Jiayi Li [1], Yuchen Qiu [1], Zhenwei Shi [4] and Yuanheng Sun [5,*]

1   School of Environmental Science and Engineering, Tiangong University, Tianjin 300387, China; zhangzhaoxu@tiangong.edu.cn (Z.Z.); 2113620105@tiangong.edu.cn (S.F.); 2213620136@tiangong.edu.cn (J.L.)
2   The Eighth Geological Brigade, Hebei Bureau of Geology and Mineral Resources Exploration, Qinhuangdao 066000, China
3   Marine Ecological Restoration and Smart Ocean Engineering Research Center of Hebei Province, Qinhuangdao 066000, China
4   Key Laboratory of Technology in Geo-Spatial Information Processing and Application System, Chinese Academy of Sciences, Beijing 100190, China; shizw@aircas.ac.cn
5   Environmental Information Institute, Navigation College, Dalian Maritime University, Dalian 116026, China
*   Correspondence: yhsun@dlmu.edu.cn

Abstract: With burgeoning economic development, a surging influx of greenhouse gases, notably carbon dioxide (CO_2), has precipitated global warming, thus accentuating the critical imperatives of monitoring and predicting carbon emissions. Conventional approaches employed in the examination of carbon emissions predominantly rely on energy statistics procured from the National Bureau of Statistics and local statistical bureaus. However, these conventional data sources, often encapsulated in statistical yearbooks, exclusively furnish insights into energy consumption at the national and provincial levels, so the assessment at a more granular scale, such as the municipal and county levels, poses a formidable challenge. This study, using nighttime light data and statistics records spanning from 2000 to 2019, undertook a comparative analysis, scrutinizing various modeling methodologies, encompassing linear, exponential, and logarithmic models, with the aim of assessing carbon emissions across diverse spatial scales. A multifaceted analysis unfolded, delving into the key attributes of China's carbon emissions, spanning total carbon emissions, per capita carbon emissions, and carbon emission intensity. Spatial considerations were also paramount, encompassing an examination of carbon emissions across provincial, municipal, and county scales, as well as an intricate exploration of spatial patterns, including the displacement of the center of gravity and the application of trend analyses. These multifaceted analyses collectively contributed to the endeavor of predicting China's future carbon emission trajectory. The findings of the study revealed that at the national scale, total carbon emissions exhibited an annual increment throughout the period spanning 2000 to 2019. Secondly, upon an in-depth evaluation of model fitting, it was evident that the logarithmic model emerged as the most adept in terms of fitting, presenting a mean R^2 value of 0.83. Thirdly, the gravity center of carbon emissions in China was situated within Henan Province, and there was a discernible overall shift towards the southwest. In 2025 and 2030, it is anticipated that the average quantum of China's carbon emissions will reach 7.82×10^2 million and 25.61×10^2 million metric tons, with Shandong Province emerging as the foremost contributor. In summary, this research serves as a robust factual underpinning and an indispensable reference point for advancing the scientific underpinnings of China's transition to a low-carbon economy and the judicious formulation of policies governing carbon emissions.

Keywords: nighttime light; carbon emission; spatiotemporal analysis; scale; prediction

1. Introduction

Today's society faces various challenges and threats, such as resource constraints, energy depletion, reduced food production, environmental pollution, overpopulation, and global warming [1–3]. Amongst them, global warming has emerged as the most critical issue, directly impacting the natural environment and the sustainable development of human society and economy [4]. The factors that affect global warming are natural [5], such as solar radiation, atmospheric radiation, and atmospheric circulation, and anthropogenic [6,7]. The predominant contributor to the rise in global temperatures and global warming is large-scale human activities that emit substantial amounts of greenhouse gases, such as CO_2, into the atmosphere [8,9]. These greenhouse gases are highly transmissive of solar radiation and highly absorbent of longwave radiation reflected from the Earth's surface, leading to an increase in global temperature, a phenomenon known as the greenhouse effect [10,11]. The latest assessment by the Intergovernmental Panel on Climate Change shows that the global average temperature increased by 1.09 °C from the second half of the 19th century to the first decades of the 21st century [12]. The main reason is the increased concentration of CO_2. Carbon emissions have become a focus of interest for all countries, and the study of carbon emissions has garnered global attention, progressively becoming a topic of international concern [13].

As China experiences rapid industrialization and urbanization, and with its economic development heavily reliant on fossil energy, the country has generated significant carbon emissions [14]. China has become the country with the highest CO_2 emission in the world, and its share of CO_2 emissions has increased from 10.9% in 1990 to 28.61% in 2018 [15]. To control energy consumption and reduce CO_2 emissions, China has established corresponding targets and policies. Notably, the emission reduction targets for 2030 stipulate that carbon emissions will peak by that year, and non-fossil energy will constitute 20% of total energy consumption [16]. Concurrently, the Chinese government plans to peak carbon emissions around 2030 [17]. Against this backdrop, China has proposed the dual carbon goals of achieving carbon peaking and carbon neutrality, aligning with the demands of the current era [18].

Against the backdrop of frequent global warming and environmental issues, remote sensing technology offers several advantages, including easy accessibility, rapid updates, and extensive coverage [19]. Consequently, remote sensing plays a pivotal role in monitoring greenhouse gases and atmospheric pollutants [20]. (1) Direct calculation is based on greenhouse gas remote sensing satellites and data [21]. The monitoring technology of these satellites quantifies greenhouse gas concentrations through non-contact methods involving various technologies such as Fourier transform infrared spectroscopy (FTIR), differential absorption lidar (DIAL), laser heterodyne spectroscopy (LHS), and spatial heterodyne spectroscopy (SHS) [22]. (2) Remote sensing observations are used for indirect accounting and inversion of greenhouse gases [23]. Currently, optimal estimation methods and differential optical absorption spectroscopy (DOAS)-related algorithms are the mainstream approaches for estimating non-CO_2 gas concentrations from satellite observations. The column concentration accuracy can reach 1% for CH_4, 10% for NO_2, 1% for N_2O, and 1% for O_3. (3) In the monitoring of atmospheric pollution particles based on remote sensing data [24], a three-dimensional monitoring network for urban air pollution is built based on ground environmental air automatic monitoring stations, and the environmental quality of the entire region is simulated and analyzed using measured data from the stations [25]. This network facilitates the simulation and analysis of regional environmental quality using measured data from stations, including inhalable particulate matter, fine particulate matter, nitrogen dioxide, sulfur dioxide, carbon monoxide, and ozone. In summary, remote sensing technology plays a crucial role in various aspects of atmospheric environment monitoring such as trace gases, atmospheric particulate matter, volatile organic compounds (VOCs), and hazardous substances [26].

In China, CO_2 emissions are generally quantified using energy statistics [13]. The country's vast territory and regional disparities make the collection of energy statistics burdensome and complex [27]. Meanwhile, China's research on carbon emissions is mainly based on energy statistics from the National Bureau of Statistics and local statistical bureaus. However, statistical yearbooks only provide energy consumption data at the national and provincial levels. Data on the energy consumption of the country's prefectural cities at county and township levels and even smaller scales are unavailable, so research cannot be conducted on carbon emissions at small scales [28]. Furthermore, the quality of data statistics varies across different regions of China, and energy consumption statistics in national and local energy statistical yearbooks are lagging [29].

With the advancement of remote sensing technology, the use of satellite data to measure carbon emissions is gaining momentum [30]. Remote sensing technology enables the periodic and rapid acquisition of macro-level information with minimal data constraints [31,32]. Therefore, this technology is widely used in related fields, such as agriculture and forestry monitoring, weather and meteorological forecasting, hydrological water monitoring, environmental monitoring, mapping and surveying, military reconnaissance, and geology and minerals [33–35]. Compared to traditional methods like statistical approaches, remote sensing technology overcomes the spatial and temporal limitations associated with data collection [32,36]. Thus, remote sensing technology provides data support for studying carbon emissions at various scales [37]. Nighttime light imagery, a special kind of remote sensing imagery, has long light sequences that effectively record light information related to human activities [38]. Consequently, nighttime light data have become a crucial source for carbon emission studies [39].

This research aims to control the total amount of carbon emissions in China and explore the patterns and development trends of energy carbon emissions. The study focuses on three main objectives: (1) Using statistical and nighttime light data from 2000 to 2019, a model for fitting carbon emissions and nighttime lighting is constructed to estimate carbon emissions at different scales (province, city, and county). This task compensates for the limitations of statistical data. (2) The basic characteristics of total carbon emissions, per capita carbon emissions, and carbon emission intensity at different scales (province, city, and county) in 2000, 2005, 2010, 2015, and 2019 are examined. Carbon emission characteristics are analyzed using spatial center of gravity migration, trend changes, and spatial aggregation methods. (3) Based on the grey prediction model GM (1, 1), provincial-scale carbon emissions for 2025 and 2030 are forecasted using carbon emission data from 2000 to 2019. This research aims to provide a reference for the scientific and sustainable development of a low-carbon economy in China and for the formulation of corresponding carbon emission reduction policies by regional governments.

2. Materials

2.1. Study Area

As the world's most populous country, China is undergoing rapidly growing urbanization as it enters the 21st century [40]. By the end of 2019, mainland China comprised 360 prefecture-level cities and 2774 county-level cities [41]. This research excludes Tibet, Hong Kong, Macau, and Taiwan due to regional differences and the unavailability of statistics in these areas (Figure 1). To align with available official statistics and to reflect the continuous changes in China's carbon emissions, the study covers a period of 20 years, from 2000 to 2019.
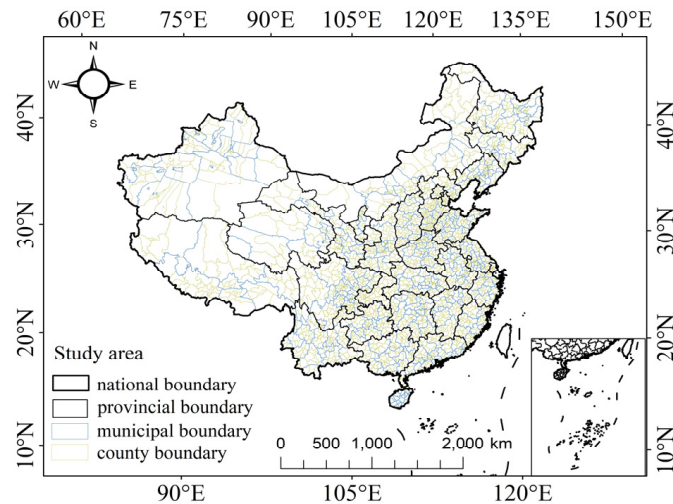
Figure 1. Research area.

2.2. Study Data

2.2.1. Nighttime Light Data

Data were obtained from the Long Time Series Nighttime Light Dataset of China (2000–2020) published by Zhong Xiaoya in the Global Change Research Data Publishing and Repository [42]. This dataset for China was based on the calibration and fusion of DMSP/OLS annual moonlight image data and NPP/VIIRS monthly image data, with a spatial resolution of 1 km. Both the oversaturation issue of DMSP/OLS data and the noise problem in NPP/VIIRS data had been addressed. The continuity and availability of the data were conducive to the extraction of information on cities and towns across the country over an extended period.

The original DMSP/OLS and NPP/VIIRS data present challenges due to variations in sensors, spatiotemporal resolutions, data processing methods, and pixel interpretations, which pose difficulties in integrating long-term nighttime lighting data. These data issues significantly constrain the potential applications of nighttime light data and may also impact the effectiveness of research relying on such data. Therefore, researchers conducted a series of data processing steps on DMSP/OLS images from 2000 to 2013 and monthly NPP/VIIRS images from 2012 to 2020. Through preprocessing, mutual correction, and saturation correction techniques applied to DMSP/OLS images, annual DMSP/OLS datasets were obtained. Simultaneously, preprocessing steps including outlier processing and median-based annual synthesis on NPP/VIIRS images were performed to obtain annual NPP/VIIRS datasets. Finally, by fusing the annual EANTLI dataset with the NPP/VIIRS dataset through spatial resolution integration, fitting function construction and continuous corrections were made resulting in long-term nighttime light datasets [42].

2.2.2. Statistical Data

To calculate carbon emissions from energy consumption at different scales (provinces, municipalities, and districts), annual statistics were obtained from the National Bureau of Statistics of the People's Republic of China. Data on 11 energy sources were collected based on the China Energy Statistical Yearbook from 2000 to 2019, as well as from provincial and local energy balances (including autonomous regions and municipalities directly under the central government, but excluding Tibet, Taiwan, Hong Kong, and Macao) from the relevant city statistics. Additionally, the carbon emission factors for different energy sources were derived from the IPCC Guidelines for National Greenhouse Gas Inventories.

3. Methods

Figure 2 illustrates the technical route of this study, which encompasses the following: (1) data collection and processing; (2) carbon emission model construction and comparison; (3) application of the results, which mainly includes carbon emission analysis at different scales, pattern analysis, and center of gravity analysis; and (4) prediction of carbon emissions for the years 2025 and 2030 using the grey model.
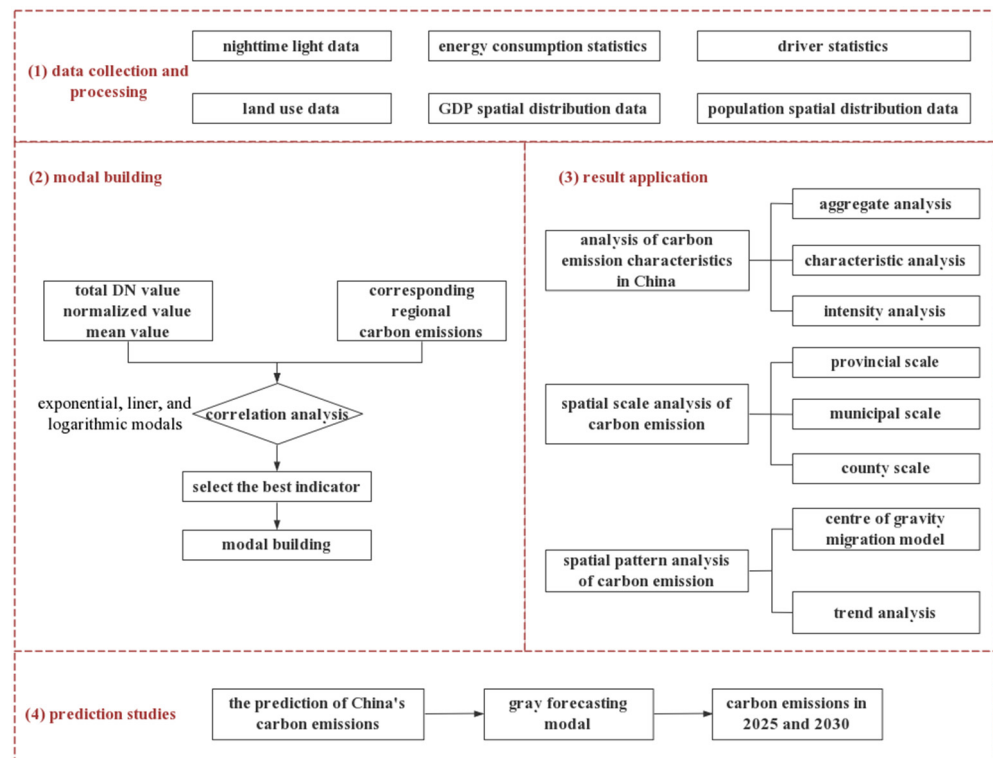

Figure 2. The flowchart of this study.

3.1. Carbon Emission Modeling

3.1.1. Accounting for Energy Carbon Emissions in China

To calculate China's carbon emissions from energy consumption, the most authoritative international carbon emission calculation method was used in this study. To calculate the total amount of carbon emissions from each variety of energy sources, this method was to convert the total consumption of various energy sources into the consumption of standard coal by folding the standard coal coefficient, and then use the standard coal multiplied by the respective carbon emission coefficients [43]. The CO_2 emissions are calculated using the following formula:

$$E = \sum_{i=1}^{j} EN_i \times EF_i \times \frac{44}{12} \tag{1}$$

where E is the emission of CO_2 from j energy sources ($\times 10^4$ t), EN_i is the energy consumption of the energy source category ($\times 10^4$ t), EF_i is the carbon emission factor of the energy source category, i is the type of energy source, and j is the number of energy sources.

The energy types, reference coefficient of standard coal, and carbon emission coefficients are shown in Table 1.

Table 1. The energy types, reference coefficient of standard coal, and carbon emission coefficients.

Type of Energy	Reference Coefficient of Standard Coal (kJ/kg)	Carbon Emission Coefficients
raw coal	0.7143	0.7559
refined coal	0.7143	0.9000
coke (processed coal used in blast furnace)	0.9714	0.8550
coke oven gas	0.6143	0.3548
crude oil	1.4286	0.5857
petrol	1.4714	0.5538
diesel	1.4714	0.5714
diesel oil	1.4571	0.5921
fuel oil	1.4286	0.6185
liquefied petroleum gas	1.7143	0.5042
refinery dry gas	1.5714	0.4602
petroleum	1.3300	0.4483

3.1.2. Extraction of DN Values

Extensive research has shown that the total nighttime light intensity value (T) and carbon emissions have a good correlation [44]. T is the sum of DN values in a region. In this study, the indicator of total T in the study area was selected to fit the energy carbon emissions. The image element values of EANTLI nighttime lighting data were extracted using the provincial administrative boundaries from 2000 to 2019. The T-value of the study area was calculated subsequently. The T-value is calculated using the following formula:

$$T = \sum_{i=0}^{n} DN_i \tag{2}$$

where DN_i is the value of the image element in region i and n is the number of image elements.

3.1.3. Model Calculations at Different Scales

In this study, exponential, linear, and logarithmic models were constructed. The best model was selected to achieve the calculation of carbon emissions at different scales using the coefficient of determination (R^2). In the fitting comparison, the correlation coefficients of the exponential, linear, and logarithmic models were very high (R^2 were all more than 0.7). Among them, the logarithmic fit was the best, and the mean value of R^2 was 0.83. To calculate and convert the sum of carbon dioxide emissions and DN values, the logarithmic model was selected in this study. The constructed model was calculated using the following formula:

The provincial conversion model is as follows:

$$E_{ij} = K \times \ln(T_{ij}) - B \tag{3}$$

The downscaled municipal and county conversion model is as follows:

$$E_{ij} = \frac{T_{kj}}{T_{ij}} K \times \ln(T_{ij}) - B \tag{4}$$

where E_{ij} is the carbon emissions of province i in year j, T_{kj} is the total value of city and county k in year j, T_{ij} is the total value of nighttime light, K is the provincial simulation coefficient, and B is the simulation intercept.

3.2. Correlation Analysis

The Pearson correlation coefficient (R) can reflect the degree and direction of correlation between two variables [45]. In this study, the correlation coefficient between the total intensity value of nighttime lighting and carbon emissions from energy consumption from 2000 to 2019 was calculated. The correlation coefficient calculation formula is as follows:

$$R = \frac{\sum\limits_{i=1}^{n} \left(X_i - \overline{X}\right)\left(Y_i - \overline{Y}\right)}{\sqrt{\sum\limits_{i=1}^{n} \left(X_i - \overline{X}\right)^2 \left(Y_i - \overline{Y}\right)^2}} \tag{5}$$

where R is the correlation coefficient, n is the length of the time series, X is the monthly average total intensity value of night lights, and Y is the carbon emission value of energy consumption.

3.3. Center of Gravity Migration Model

The concept of the center of gravity migration model comes from mechanics in physics and represents a mathematical weighted average. Its application to geography began with calculating the population center of gravity, expressed through latitude and longitude coordinates. By using a migration model based on the center of gravity, we could simulate temporal changes in carbon emissions' center of gravity, providing a more intuitive representation of their spatial and temporal dynamics within the study area [46]. To investigate China's changing carbon emissions patterns, this model was used to calculate the carbon emissions' center of gravity between 2000 and 2019. The center of gravity migration model is the following formulas:

$$\overline{X}_t = \frac{\sum\limits_{i=1}^{n} E_{it} x_{it}}{\sum\limits_{i=1}^{n} E_{it}} \tag{6}$$

$$\overline{Y}_t = \frac{\sum\limits_{i=1}^{n} E_{it} y_{it}}{\sum\limits_{i=1}^{n} E_{it}} \tag{7}$$

where $\overline{X}_t$ is the latitude of the center of gravity of China's carbon emissions in year t, $\overline{Y}_t$ is the longitude of the center of gravity of China's carbon emissions in year t, E_{it} is the carbon emissions on grid i in year t, x_{it} is the latitude coordinate of the center of grid i in year t, and y_{it} is the longitude coordinate of the center of grid i in year t.

3.4. Trend Analysis

Trend analysis is a method of predicting the trend of a variable over time by performing a linear regression analysis [45]. To analyze the growth trend of carbon emissions in different regions, the following formula is used to calculate the trend (slope) of carbon emissions:

$$slope = \frac{n \times \sum\limits_{i=1}^{n} x_i t_i - \left(\sum\limits_{i=1}^{n} x_i\right)\left(\sum\limits_{i=1}^{n} t_i\right)}{n \times \sum\limits_{i=1}^{n} t_i^2 - \left(\sum\limits_{i=1}^{n} t_i\right)^2} \tag{8}$$

where slope is the trend in carbon emissions, x_i is the scaled exponential value, n is the length of the study period, and t_i is the year from 2000 to 2019. Positive slope values indicate an increase in carbon emissions, while negative slope values indicate a decrease. Therefore, the slope value can display the trend of carbon emissions during the study period. To further classify carbon emissions, trends were categorized into more refined

levels including negative growth type, slow growth, slower growth, medium growth, faster growth, and rapid growth. The specific classification standards are shown in Table 2. x is the average value of the slope, and s is the standard deviation.

Table 2. Criteria for classifying the type of growth in carbon emissions.

Type of Carbon Growth	Delineation Criterion
negative growth	slope < 0
slow growth	$0 \leq$ slope < x~0.5 s
slower growth	x~0.5 s $\leq$ slope < x + 0.5 s
medium growth	x + 0.5 s $\leq$ slope < x + 1.5 s
faster growth	x + 1.5 s $\leq$ slope < x + 2.5 s
rapid growth	slope $\geq$ x + 2.5 s

3.5. Predictive Modeling

Grey theory posits that all random variables are grey quantities and grey processes that change within a certain range and over a certain period. Data processing does not aim to establish the statistical law and probability distribution of data; it processes the original data so that they become regular time series data, on the basis of which a mathematical model is established. The GM series model is the basic model of grey prediction theory. In particular, the GM (1, 1) model is widely used in the field of predicting carbon emissions [47]. The GM (1, 1) is as follows:

Suppose $X^{(0)}$ as a time sequence:

$$X^{(0)} = (x^{(0)}(1), x^{(0)}(2), \cdots, x^{(0)}(n)) \tag{9}$$

where $X^{(0)}$ is a nonnegative series

$$X^{(0)} = (x^{(0)}(1), x^{(0)}(2), \cdots, x^{(0)}(n)) \tag{10}$$

where $x^{(0)}(k) \geq 0$, $k = 1, 2, \cdots, n$.

$X^{(1)}$ can be obtained as 1-AGO series of $X^{(0)}$:

$$X^{(1)} = (x^{(1)}(1), x^{(1)}(2), \cdots, x^{(1)}(n)) \tag{11}$$

where $x^{(1)}(k) = \sum_{i=1}^{k} x^{(0)}(i)$, $k = 1, 2, \cdots, n$.

$Z^{(1)}$ is the adjacent mean value generation sequence of $X^{(1)}$, also called the background value:

$$Z^{(1)} = (z^{(1)}(2), z^{(1)}(3), \cdots, z^{(1)}(n)) \tag{12}$$

where $z^{(1)}(k) = 0.5x^{(1)}(k) + 0.5x^{(1)}(k-1)$, $k = 2, 3, \cdots, n$.

The basic form of the GM (1, 1) model can be defined as

$$x^{(0)}(k) + az^{(1)}(k) = b \tag{13}$$

The grey model can be written as the matrix form:

$$Y = B\hat{a} \tag{14}$$

Applying the least squares method, the estimated coefficients $[a, b]^T$ can be calculated as

$$Y = \begin{bmatrix} x^{(0)}(2) \\ x^{(0)}(3) \\ \vdots \\ x^{(0)}(n) \end{bmatrix} \quad B = \begin{bmatrix} -z^{(1)}(2) & 1 \\ -z^{(1)}(3) & 1 \\ \vdots & \vdots \\ -z^{(1)}(n) & 1 \end{bmatrix} \quad \hat{a} = \begin{bmatrix} a \\ b \end{bmatrix} \tag{15}$$

The whitening equation is defined as

$$\frac{\mathrm{d}x^{(1)}}{\mathrm{d}t} + \mathrm{a}x^{(1)} = b \tag{16}$$

With $x^{(1)}(1) = x^{(0)}(1)$, the predicted value $\hat{x}^{(1)}(k+1)$ is calculated as

$$\hat{x}^{(1)}(k+1) = \left(x^{(1)}(0) - \frac{b}{a}\right)e^{-ak} + \frac{b}{a} \quad (k = 1, 2, \cdots, n) \tag{17}$$

4. Results

This section primarily presents the results and application analysis of carbon emission calculation, aiming to explore the characteristics of China's carbon emissions from 2000 to 2019. Firstly, we conducted calculations for total carbon emissions, per capita carbon emissions, and carbon emission intensity to analyze their respective characteristics. Secondly, models were developed to calculate total carbon emissions at various scales, including provinces, cities, and counties. Additionally, per capita carbon emissions and provincial-level carbon emission intensity were calculated to conduct a spatial scale analysis of China's carbon emissions. Lastly, through the utilization of a shift-of-focus model along with trend analysis and prediction techniques for carbon emission data, the spatial pattern of China's carbon emissions was analyzed while its spatiotemporal dynamic changes were also studied.

4.1. Carbon Emission Calculation Based on Statistical Data
4.1.1. National-Scale Carbon Emission Calculation

A.   National-scale carbon emissions

The total amount of carbon emissions from energy emissions in China is depicted in Figure 3. From 2000 to 2019, with the exception of 2015, there was a consistent increase in total carbon emissions, escalating from 4.42 Gt in 2000 to 15.83 Gt in 2019. The average annual growth rate during this period was 7.08%. Notably, the growth rate was more rapid between 2003 and 2006, and again in 2013, with an average annual growth rate of approximately 14.56%. The highest growth rate recorded was observed in the year 2004, reaching 17.36%. Subsequently, carbon emissions exhibited a slower pace of growth from 2014 to 2019, with an average annual growth rate of 1.44%. In 2015, there was a notable decline, with a negative growth rate of −1.06%.
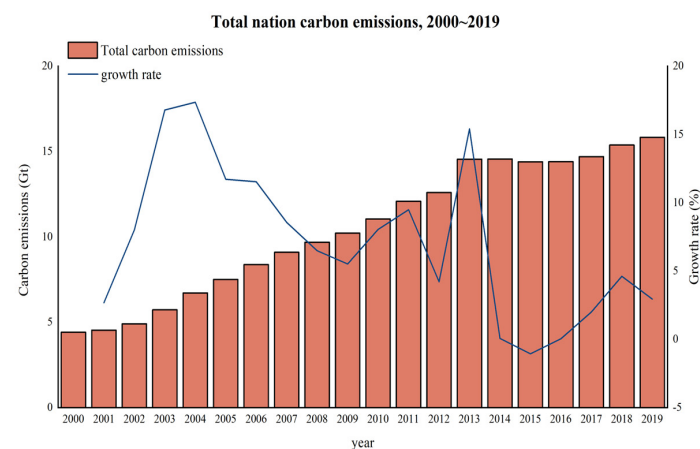

Figure 3. Total national carbon emissions and growth rate, 2000 to 2019.

B.   National-scale per capita carbon emissions

China's per capita carbon emissions are presented in Figure 4. Per capita carbon emissions indicated an increasing trend from 2000 to 2019. In 2000, the per capita carbon

emissions were 3.49 tons per person, which rose to 11.23 tons per person by 2019. The average annual growth rate during this period was 6.48%. Notably, positive growth rates were recorded from 2000 to 2013 and from 2017 to 2020, with an average annual growth rate of approximately 7.87%. The highest growth rate occurred in the year 2004 (16.67%). Conversely, negative growth rates were observed from 2014 to 2016, resulting in an average annual decline of −0.92%. The largest negative growth rate was registered in the year 2015 (−1.55%).
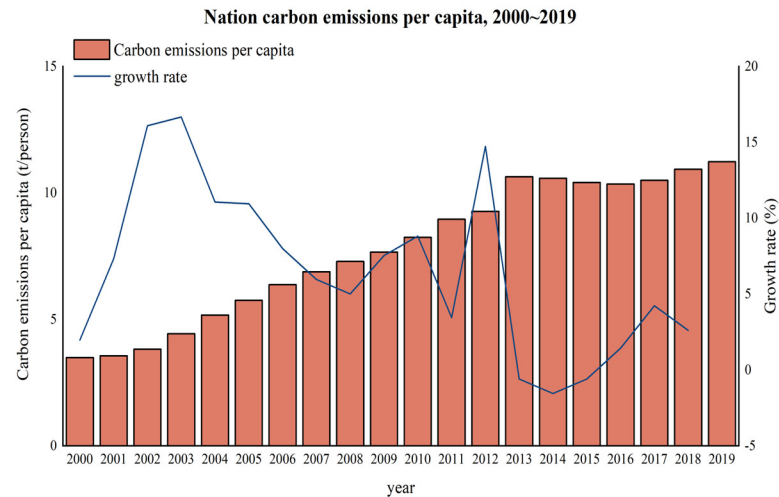
Nation carbon emissions per capita, 2000~2019

Figure 4. Total national per capita carbon emissions and growth rates, 2000 to 2019.

C.   National-scale carbon emission intensity

The term "carbon emission intensity" is defined as the amount of carbon emitted per unit of economic output, where higher carbon intensity indicates less efficient energy use and greater utilization of energy and other resources for the same level of output. In practical research, carbon emissions per unit of gross national product are often utilized to calculate intensity values. Figure 5 illustrates China's national carbon emission intensity and its growth rate from 2000 to 2019. During this period, China experienced a downward trend in carbon emission intensity, with a decrease in total emissions from 4.41 tons per CNY 10,000 to 1.60 tons per CNY 10,000. This corresponded to an average annual reduction rate of 5.09%. These findings signify a notable decline in China's carbon emission intensity over the study period, largely attributable to its economic development.
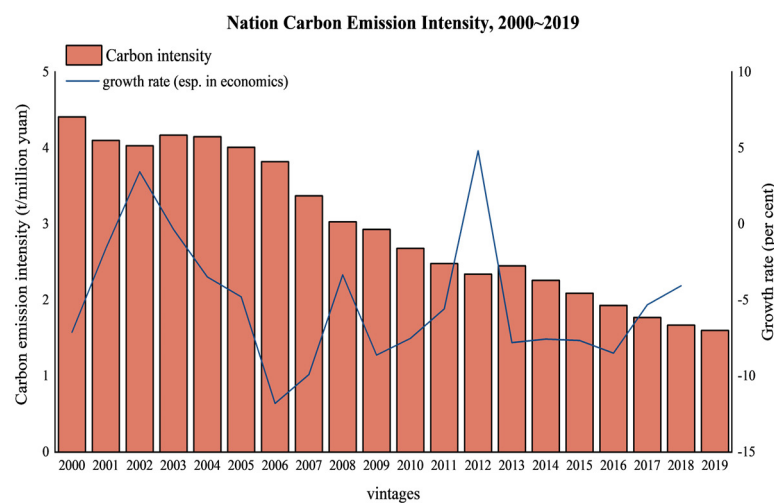
Nation Carbon Emission Intensity, 2000~2019

Figure 5. National carbon emission intensity and growth rate, 2000 to 2019.

4.1.2. Provincial-Scale Carbon Emission Calculation

A.   Correlation analysis between nighttime lighting and carbon emissions at the provincial scale

To choose a more effective indicator from night light data to fit carbon emissions, this study used the total T-value for correlation with the calculated carbon emission data of each administrative district. The results of this correlation, measured by the Pearson correlation coefficient (R), between the total T-value and carbon emissions are presented in Table 3.

Table 3. Pearson's correlation coefficients between total T-value and carbon emissions.

Provinces	R	Provinces	R
Beijing	0.875	Henan	0.824
Tianjin	0.925	Hubei	0.835
Hebei	0.919	Hunan	0.779
Shanxi	0.856	Guangdong	0.955
Inner Mongolia	0.777	Guangxi	0.949
Liaoning	0.916	Hainan	0.927
Jilin	0.838	Chongqing	0.798
Heilongjiang	0.403	Sichuan	0.771
Shanghai	0.885	Guizhou	0.832
Jiangsu	0.980	Yunnan	0.803
Zhejiang	0.910	Shanxi	0.992
Anhui	0.965	Gansu	0.977
Fujian	0.931	Qinghai	0.966
Jiangxi	0.950	Ningxia	0.950
Shandong	0.879	Xinjiang	0.962
average value	0.878		
variance	0.012		

The correlation between the total T-value and carbon emissions at the province level not only passed the significance level test but also had a high average R-value of 0.878 with a minor variation of 0.012. Except for Heilongjiang, every province had an R-value greater than 0.7. The regions with R-values above 0.9 were Tianjin, Hebei, Liaoning, Jiangsu, Zhejiang, Anhui, Guangdong, Guangxi, Hainan, Shaanxi, Gansu, Qinghai, Ningxia, and Xinjiang. These results indicate a robust connection between the T-value and overall carbon emissions, suggesting the feasibility of estimating China's carbon emissions from its nighttime lighting data.

Owing to the large size of China and the pronounced regional variations in resources, climate, and economics between provinces, three models (logarithmic, exponential, and linear models) were compared to determine the best fit. Ultimately, DN values and the overall carbon dioxide emissions at the province level were computed and fitted. Figure 6 illustrates the fitting impacts of various function models.
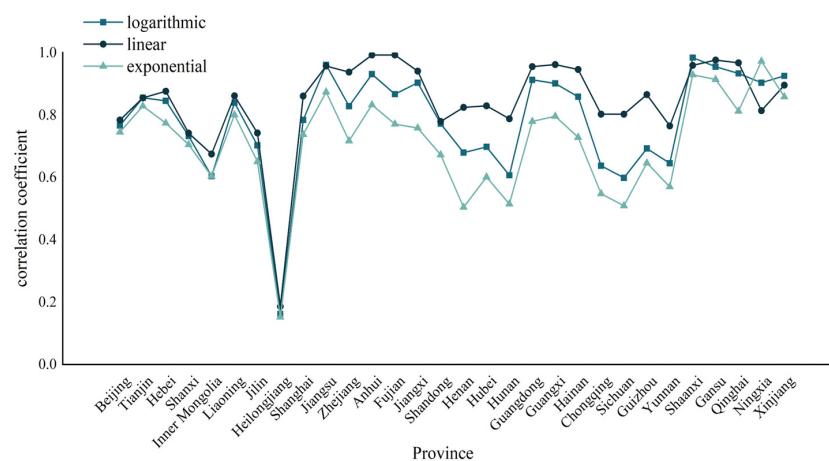

Figure 6. Correlation coefficients fitted by different models (logarithmic, linear, exponential).

In the fitting comparison, the correlation coefficients of the exponential, linear, and logarithmic models were relatively high, with the mean value of their R^2 being more than 0.7. The logarithmic model had the best fitting effect, and the mean value of R^2 was 0.83. Therefore, the logarithmic model was chosen as the calculation model for carbon emissions at the provincial-, municipal-, and county-level scales. The parameters of the logarithmic model for each province are shown in Table 4.

Table 4. Results of logarithmic fitted equations by province.

Province	K	B	R^2	Province	K	B	R^2
Beijing	10,323	−123,246	0.784	Henan	44,159	−549,038	0.824
Tianjin	18,796	−229,368	0.855	Hubei	20,609	−234,537	0.829
Hebei	96,166	−1,000,000	0.876	Hunan	15,023	−162,156	0.788
Shanxi	97,614	−1,000,000	0.742	Guangdong	97,592	−1,000,000	0.955
Inner Mongolia	68,284	−849,388	0.675	Guangxi	15,718	−182,095	0.962
Liaoning	69,561	−891,158	0.861	Hainan	4930	−52,555	0.946
Jilin	22,061	−264,133	0.742	Chongqing	6937.1	−70,012	0.803
Heilongjiang	15,572	−176,999	0.186	Sichuan	13,922	−149,693	0.803
Shanghai	14,669	−169,436	0.861	Guizhou	7679.2	−67,440	0.865
Jiangsu	56,584	−744,330	0.957	Yunnan	12,616	−141,700	0.765
Zhejiang	27,813	−343,871	0.938	Shaanxi	35,147	−431,815	0.959
Anhui	19,060	−218,990	0.992	Gansu	13,832	−155,499	0.976
Fujian	19,154	−231,076	0.992	Qinghai	5176.1	−53,851	0.967
Jiangxi	12,202	−133,406	0.941	Ningxia	16,676	−184,892	0.814
Shandong	160,087	−2,000,000	0.779	Xinjiang	58,191	−748,947	0.896

B.   Provincial-scale carbon emissions

In this study, spatial distribution maps of provincial carbon emissions in China were generated based on the logarithmic model (Figure 7). From 2000 to 2019, China's provinces had an overall trend of rising carbon emissions. China's total carbon emissions in 2000 were less than 2.0×10^2 million tons in 22 provinces. By 2005, there were only 11 provinces left. By 2010, only five provinces in China—Beijing, Chongqing, Hainan, Ningxia, and Qinghai—had carbon emissions below 2.0×10^2 million tons. The provinces of Beijing, Hainan, and Qinghai had less than 2.0×10^2 million tons by 2015. The provinces of Beijing, Chongqing, Hainan, and Qinghai fell short of this threshold by 2019. In 2010, the total carbon emissions of Shandong, Hebei, and Jiangsu amounted to 1.24×10^2, 9.40×10^2, and 8.31×10^2 million tons, respectively. The number of provinces surpassing the threshold of 8.00×10^2 million tons reached five in 2015 and increased to seven provinces by 2019. By 2019, Shandong Province exhibited the highest carbon emissions at a level of 1.77×10^2 million tons while all other provinces remained below the threshold of 1.30×10^2 million tons.

By further calculating the annual average of the total carbon emissions of each province, a bar chart depicting the average carbon emissions was generated (Figure 8). The average value of the total carbon emissions of each province was 3.84×10^2 million tons from 2000 to 2019. Shandong had the highest annual average of carbon emissions at 11.1×10^2 million tons, while Hainan had the lowest at 53.7 million tons. Zhejiang, Henan, Inner Mongolia, Guangdong, Liaoning, Shanxi, Jiangsu, Hebei, and Shandong all exceeded the average level of carbon emissions.
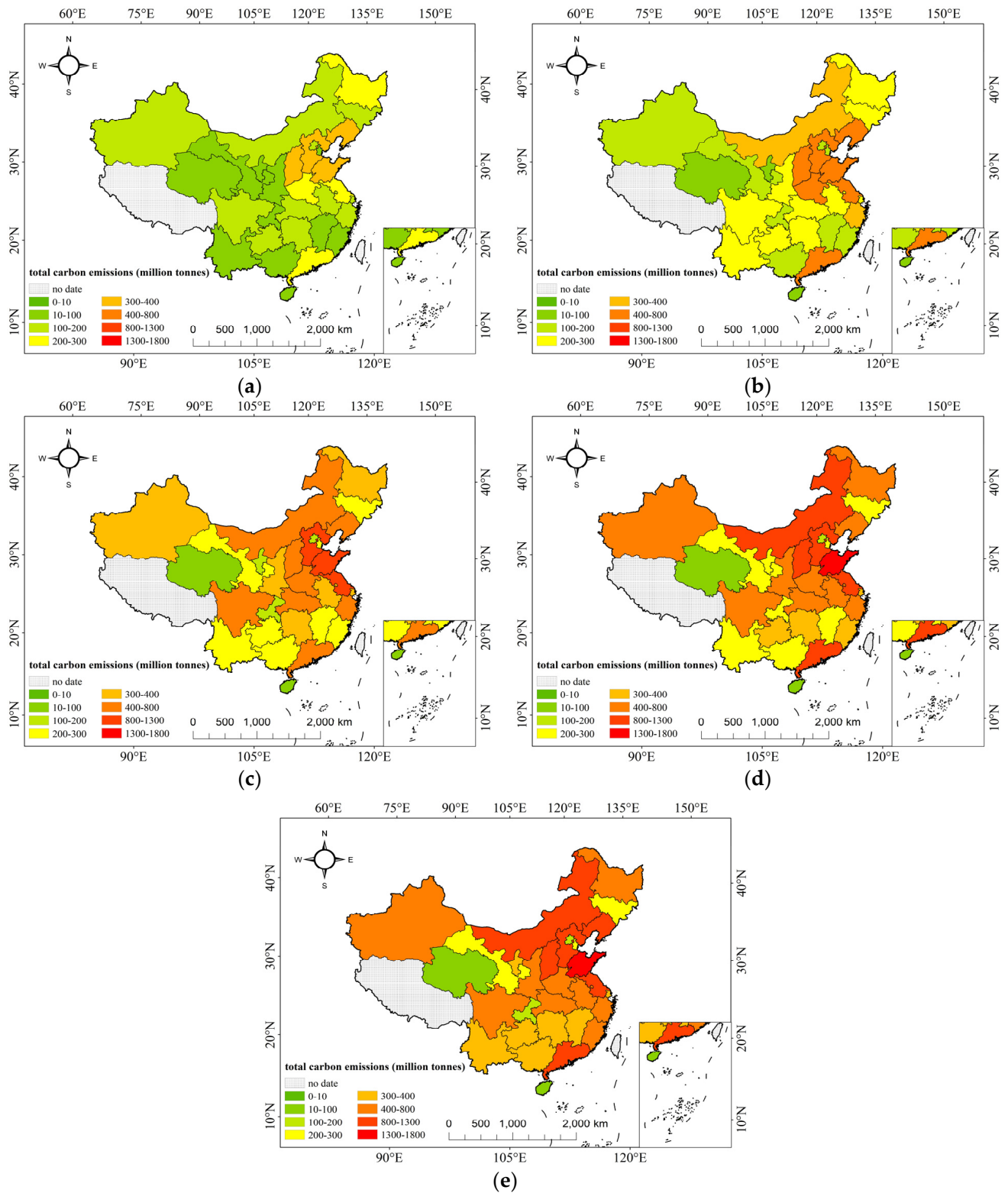
Figure 7. Provincial carbon emissions (2000, 2005, 2010, 2015, 2019). (**a**) Provincial carbon emissions in 2000. (**b**) Provincial carbon emissions in 2005. (**c**) Provincial carbon emissions in 2010. (**d**) Provincial carbon emissions in 2015. (**e**) Provincial carbon emissions in 2019.
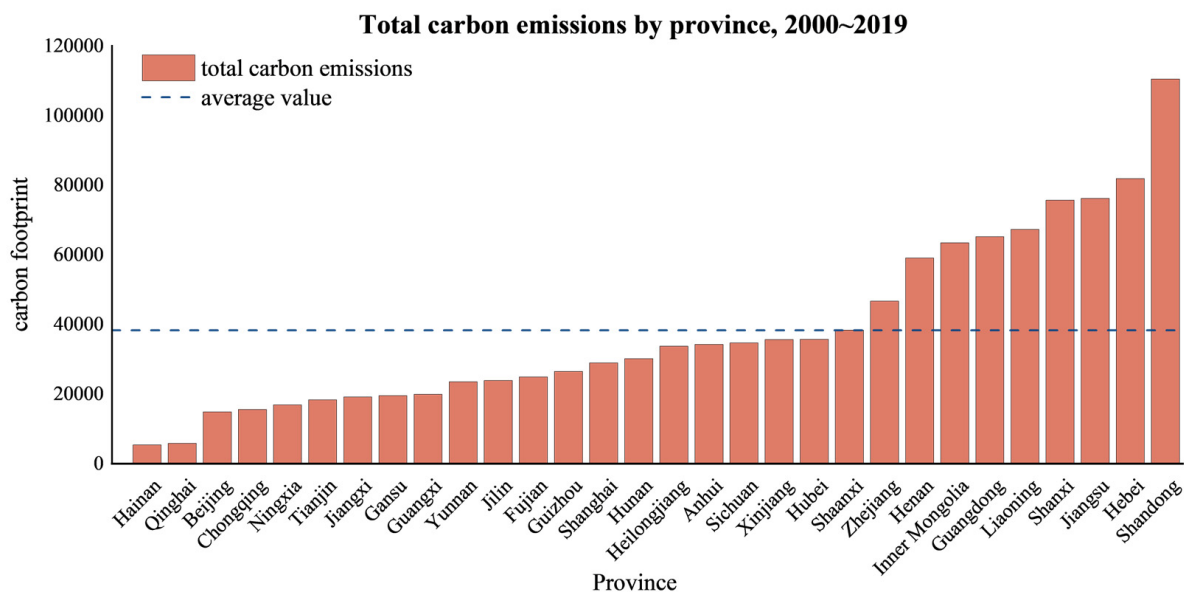
Figure 8. Average provincial carbon emissions in China (2000~2019).

C.   Provincial carbon emissions per capita

The provincial per capita carbon emissions were calculated from 2000 to 2019 (Figure 9). Overall, there was an increasing trend in provincial per capita carbon emissions during this period. In 2000, only eight provinces, namely Beijing, Tianjin, Shanghai, Heilongjiang, Jilin, Liaoning, Inner Mongolia, and Shanxi, had per capita carbon emissions of more than 5 t/person. The remaining 22 provinces had less than that amount. Shanxi had the highest per capita carbon emission at 9.86 t/person. By 2005, five provinces—Shanghai, Inner Mongolia, Shanxi, Ningxia, and Liaoning—had carbon emissions within the range of 10–20 t/person, while 11 southern regions (excluding Guizhou) still emitted less than 5 t/person. Other provinces fell between these two ranges. In 2010, the number of provinces with average per capita carbon emissions of less than 5 t/person was reduced to only two provinces, Guangxi and Jiangxi, and the per capita carbon emissions of Inner Mongolia, Ningxia, and Shanxi were greater than 20 t/person. In 2015, the per capita carbon emissions of all provinces were greater than 5 t/person, with Ningxia topping 40 t/person. The per capita carbon emissions of two provinces, Shanxi and Xinjiang, resided in the range of 30–40 t/person. The per capita carbon emissions of three provinces, namely Liaoning, Tianjin, and Shanghai, ranged between 20 and 30 t/person. Additionally, the number of provinces with per capita carbon emissions below 20 t/person decreased to 14. In 2019, the per capita carbon emissions in coastal areas exceeded 10 t/person, while the number of provinces with per capita emissions ranging from 5 to 10 t/person decreased to 10. Notably, Inner Mongolia and Ningxia exhibited significantly higher levels at 51.56 t/person and 64.39 t/person, respectively.

The histogram of the average value of per capita carbon emissions in 30 provinces from 2000 to 2019 was obtained by further calculation (Figure 10). The mean value of per capita carbon emissions across all provinces over a span of two decades was 10.29 t/person. Notably, Guangxi had the lowest per capita carbon emission at 4.17 t/person, while Ningxia recorded the highest at 27.87 t/person. Eight provinces, namely Ningxia, Inner Mongolia, Shanxi, Xinjiang, Tianjin, Liaoning, Shanghai, Shandong, Hebei, and Qinghai, had per capita carbon emissions exceeding the national average.
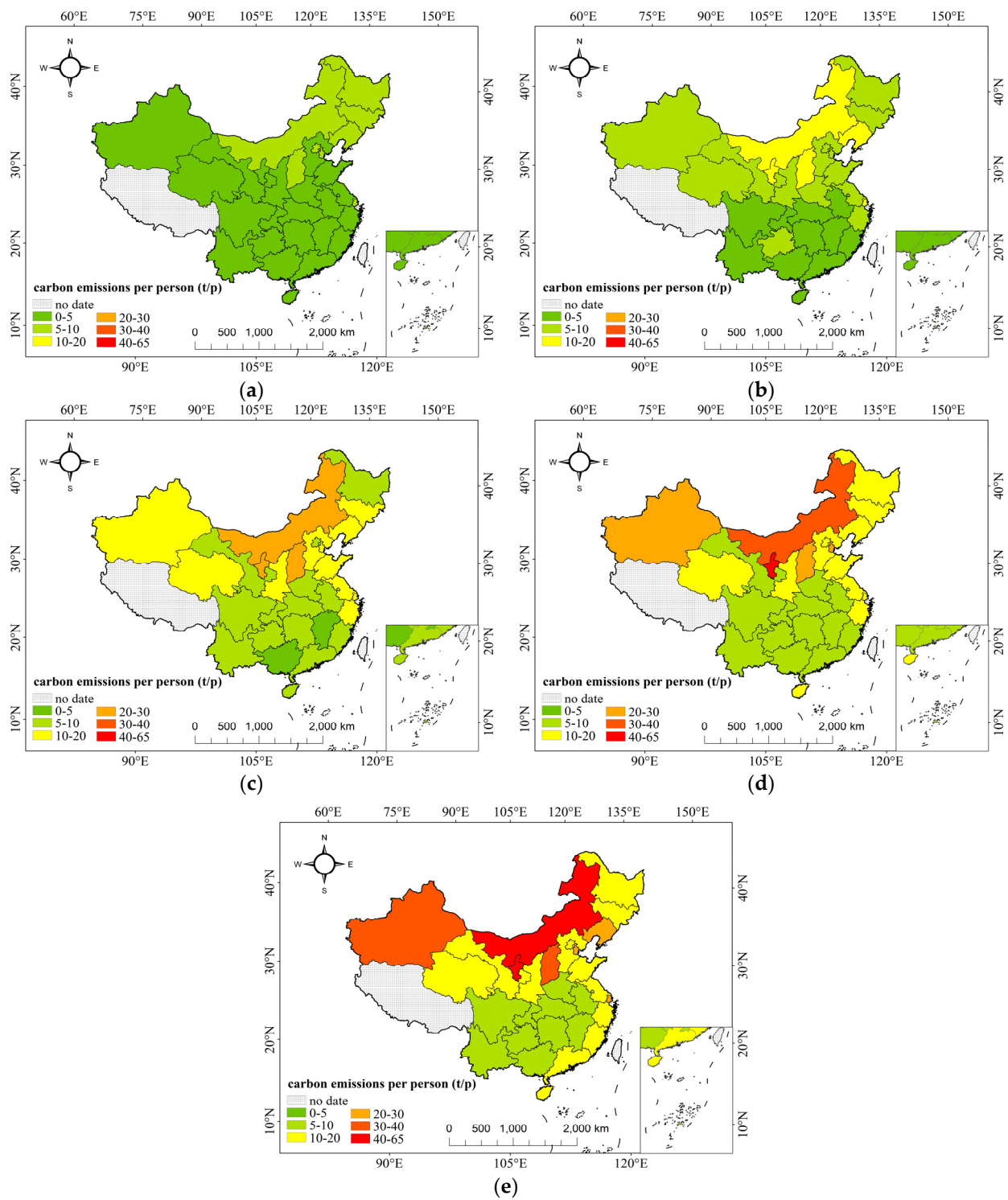
Figure 9. Carbon emissions per capita at the provincial level in China (2000, 2005, 2010, 2015, 2019). (**a**) Provincial carbon emissions per capita in 2000. (**b**) Provincial carbon emissions per capita in 2005. (**c**) Provincial carbon emissions per capita in 2010. (**d**) Provincial carbon emissions per capita in 2015. (**e**) Provincial carbon emissions per capita in 2019.
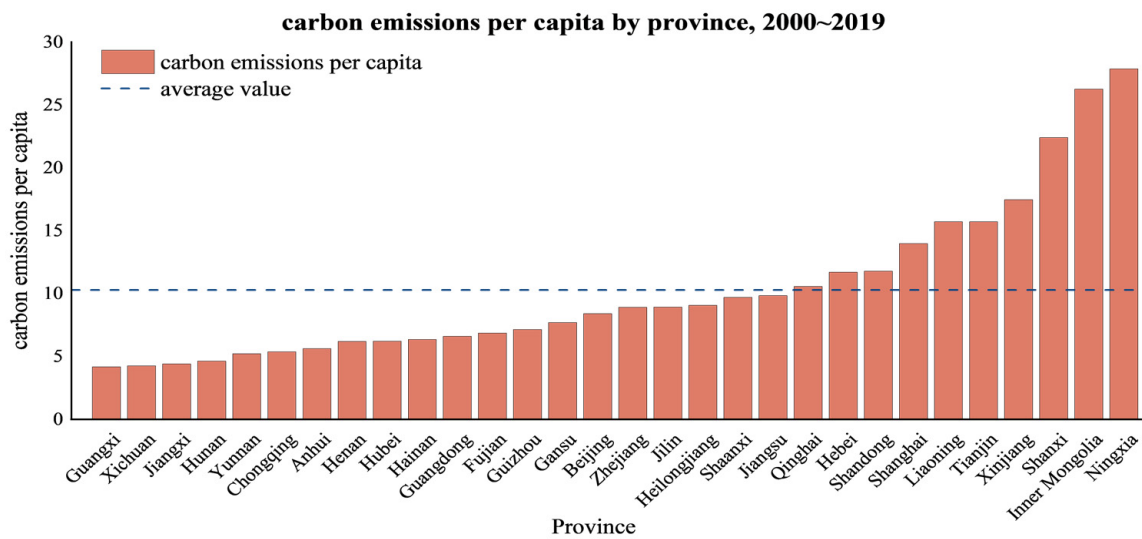
Figure 10. Average provincial per capita carbon emissions in China (2000~2019).

D.   Provincial carbon intensity

Figure 11 shows the provincial carbon emission intensity in China from 2000 to 2019. The carbon emission intensity of China's provinces exhibited a declining trend from 2000 to 2019. In 2000, Ningxia exhibited the highest carbon emission intensity at 120.91 t/CNY 10,000. The carbon emission intensity of four provinces, Shanxi, Inner Mongolia, Ningxia, and Xinjiang, was located in the range of 40–80 t/CNY 10,000. There were seven provinces located in the range of 20–40 t/CNY 10,000, namely Hebei, Liaoning, Shandong, Guizhou, Shaanxi, Gansu, and Qinghai. Three provinces, Beijing, Shanghai, and Guangdong, had carbon emission intensities below 10 t/CNY 10,000. In 2005, Ningxia still had the highest carbon emission intensity, at 41.19 t/CNY 10,000. The carbon emission intensity of three provinces, Shanxi, Inner Mongolia, and Xinjiang, decreased to 20–40 t/CNY 10,000. The provinces of Qinghai, Gansu, Shaanxi, Guizhou, Hebei, Liaoning, and Jilin exhibited a range of 10–20 t/CNY 10,000, while the remaining 19 provinces demonstrated values below 10 t/CNY 10,000. In 2010, seven provinces, Beijing, Jiangsu, Shanghai, Zhejiang, Fujian, Jiangxi, and Shandong, had a carbon emission intensity below 2 t/CNY 10,000. In 2015, 15 provinces had a carbon emission intensity of less than 1 t/CNY 10,000; 9 provinces had a carbon emission intensity between 1 and 2 t/CNY 10,000; and 6 provinces, Gansu, Ningxia, Inner Mongolia, Shanxi, Heilongjiang, and Liaoning, had a carbon emission intensity between 2 and 10 t/CNY 10,000. In 2019, only Shanxi exceeded 2 tons per CNY 10,000, while Heilongjiang, Jilin, Liaoning, and Gansu ranged from 1 to 2 tons. The other 25 provinces had intensities below 1 ton.

The average carbon emission intensity value of 30 provinces from 2000 to 2019 was obtained through further calculations (Figure 12). Over the course of 20 decades, each province exhibited an average carbon emission intensity value of 7.37 t/CNY 10,000. Among them, Beijing had the lowest carbon emission intensity of 1.60 t/CNY 10,000. Ningxia had the highest carbon emission intensity, at 28.46 t/CNY 10,000. Thirty percent of the provinces exceed the national average for all provinces, including four provinces (Ningxia, Inner Mongolia, Shanxi, and Xinjiang). The aforementioned phenomenon highlighted the necessity of enhancing energy efficiency in these provinces.
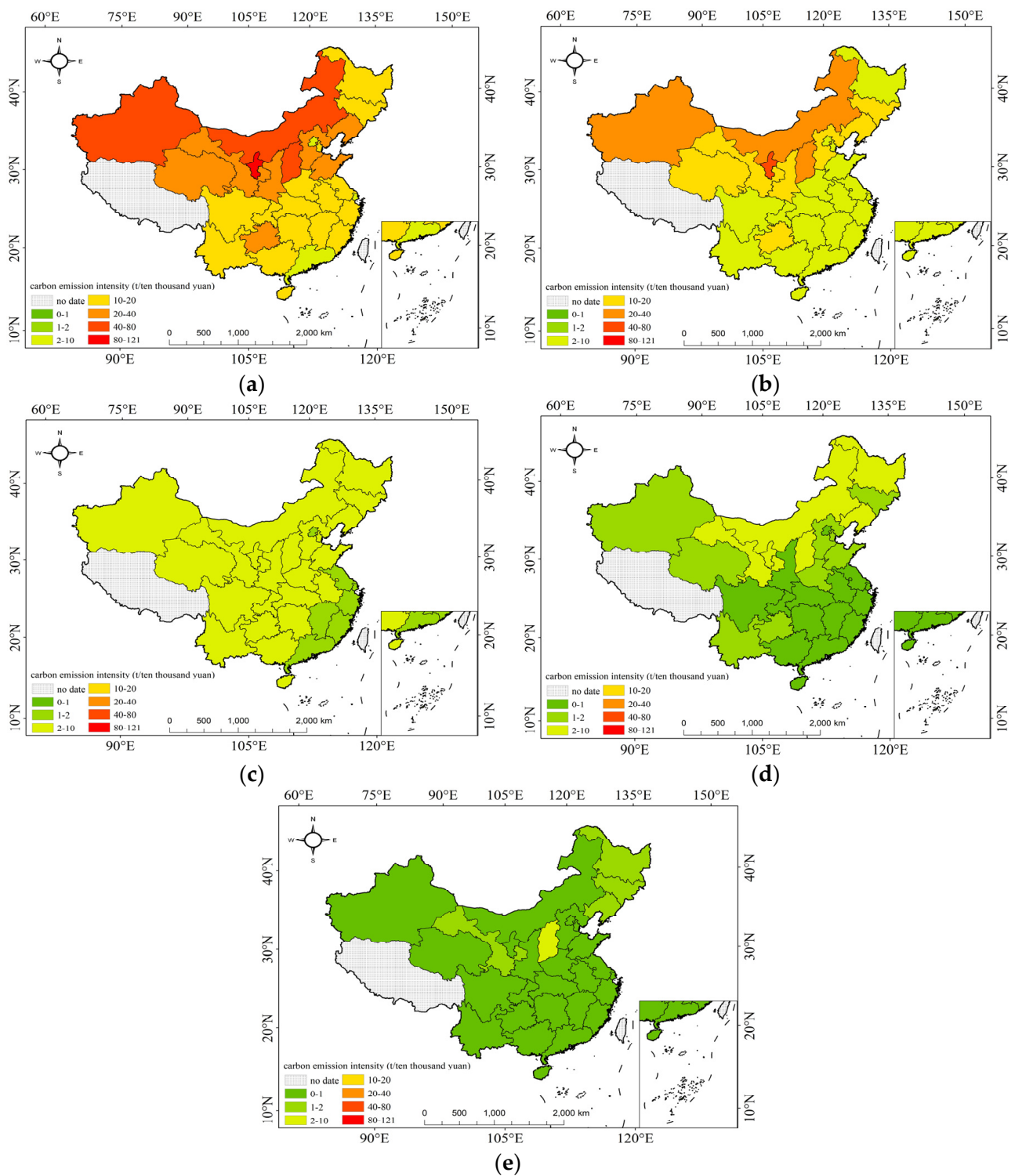
Figure 11. Provincial carbon emission intensity in China (2000, 2005, 2010, 2015, 2019). (**a**) Provincial carbon intensity, 2000. (**b**) Provincial carbon intensity, 2005. (**c**) Provincial carbon intensity in 2010. (**d**) Provincial carbon intensity, 2015. (**e**) Provincial carbon intensity in 2019.
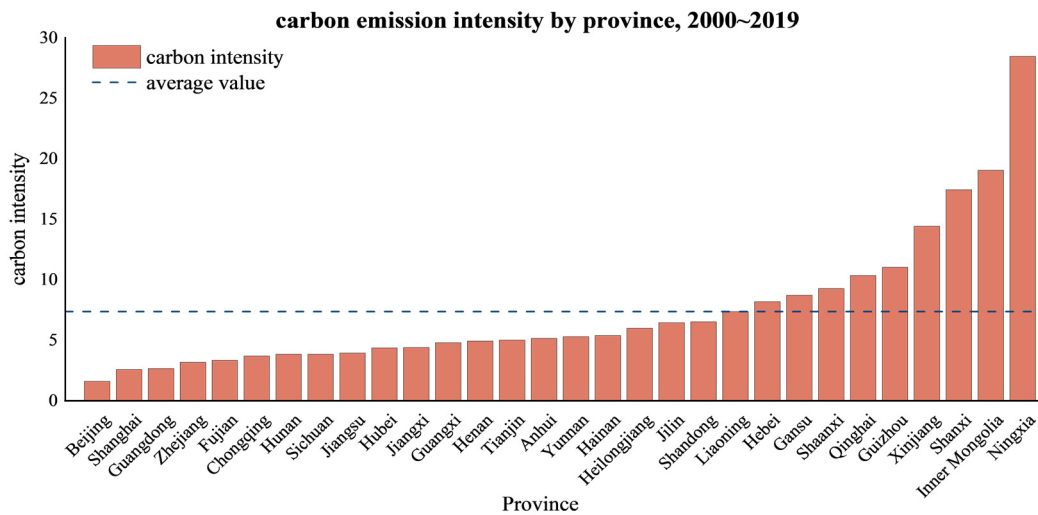
Figure 12. Provincial carbon emission intensity in China (2000~2019).

4.2. Carbon Emission Calculation Based on Remote Sensing Data of Nighttime Lighting

4.2.1. Municipal-Scale Carbon Emission Calculation

Municipal-scale carbon emission accounting was carried out based on the logarithmic model. Figure 13 displays the municipal-scale carbon emissions. The municipal-scale carbon emissions showed an increasing trend in 2000, 2005, 2010, 2015, and 2019, with mean values of 1.35×10^7 t, 2.38×10^7 t, 3.53×10^7 t, 4.15×10^7 t, and 4.71×10^7 t. Meanwhile, the carbon emissions of 30.00%, 29.17%, 30.56%, 32.50%, and 32.22% of the cities were higher than the average value. In 2000, carbon emissions below 1.5×10^7 t were observed in only 73.33% of cities, while the remaining two cities (Beijing and Shanghai) exhibited significantly higher emissions exceeding 1×10^8 t. In 2005, a decrease was noted as only 55.00% of cities had carbon emissions below 1.5×10^7 t, whereas the number of cities surpassing the threshold of 1×10^8 t rose to 13, with Shanghai accounting for emissions greater than 2×10^8 t. By 2010, less than half (40.56%) of China's cities demonstrated carbon emissions below the level of 1.5×10^7 t. Meanwhile, the number of cities with carbon emissions greater than 1×10^8 t increased rapidly to 27. Increasingly concerning trends persisted through to 2015 when approximately one-third (33.61%) of Chinese cities reported carbon emissions at or below the threshold value set at 1.5×10^7 t, while 37 cities exceeded an emission level greater than that specified by 1×10^8 t. In 2019, 29.72% of Chinese cities had carbon emissions less than 1.5×10^7 t, accounting for less than one-third, while the number of cities with carbon emissions greater than 1×10^8 t increased to 48.

Spatial analysis revealed that high-carbon-emission areas were distributed in five major regions in 2000, namely the Heilongjiang–Liaoning–Jilin, Beijing–Tianjin–Hebei, Shanghai–Nanjing–Hangzhou, Pearl River Delta, and Sichuan–Chongqing urban agglomerations. By 2005, the number of cities with high carbon emissions continued to rise within five major regions while also witnessing the emergence of high-value city clusters in areas such as Shandong Peninsula and Shanxi. In 2010, the number of high-value cities increased rapidly, with a notable concentration observed in seven specific regions: (1) Beijing–Tianjin–Hebei urban agglomerations; (2) Shandong Peninsula city cluster; (3) Chongqing and other urban agglomerations of Sichuan–Chongqing; (4) Shanghai–Nanjing–Hangzhou city cluster; (5) Ordos, Hohhot, Baotou, Yulin; (6) Changchun, Harbin, Dalian, and other urban agglomerations in Northeast China; (7) the Pearl River Delta. In 2015, some cities in Xinjiang began to show high carbon emissions, and the carbon emissions of cities in various regions of the country showed significant growth. In 2019, the number of cities with large carbon emissions continued to increase; in particular, the carbon emissions in Beijing–Tianjin–Hebei, Shandong Peninsula, Shanxi, Inner Mongolia, Erdos City, Jiangsu, and Shanghai increased more significantly.
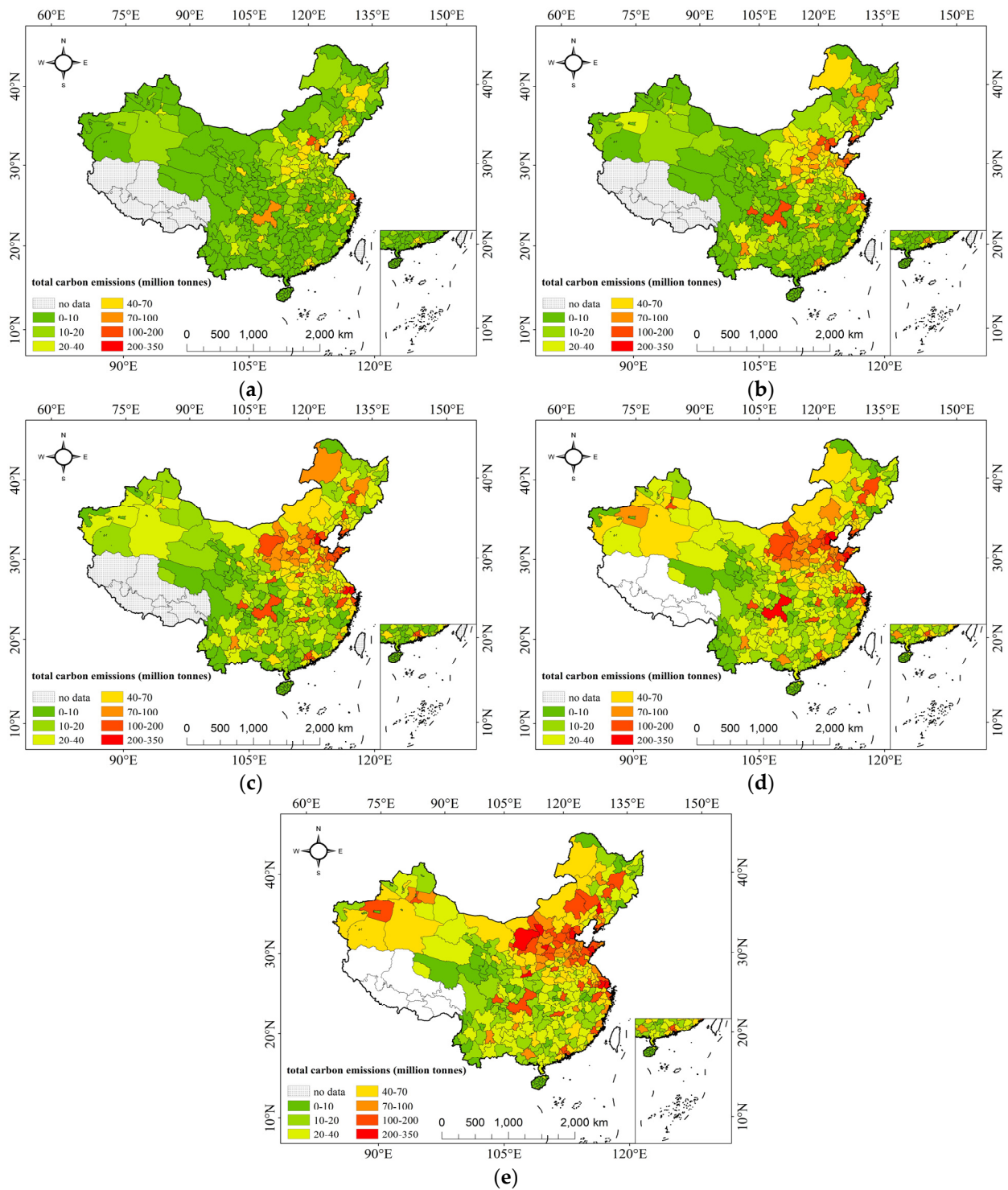
Figure 13. Municipal-scale carbon emissions (2000, 2005, 2010, 2015, 2019). (**a**) Municipal carbon emissions in 2000. (**b**) Municipal carbon emissions in 2005. (**c**) Municipal carbon emissions in 2010. (**d**) Municipal carbon emissions in 2015. (**e**) Municipal carbon emissions in 2019.

4.2.2. County-Scale Carbon Emission Calculation

County-scale carbon emission accounting was carried out based on the logarithmic model. Figure 14 shows the county-scale carbon emissions. China's county-scale carbon emissions increased in 2000, 2005, 2010, 2015, and 2019, with annual averages of 1.71×10^6 t, 3.03×10^6 t, 4.52×10^6 t, 5.32×10^6 t, and 6.04×10^6 t. In these years, the emissions of

70.21%, 69.82%, 68.73%, 69.06%, and 69.46% of counties (districts) were lower than the average value.

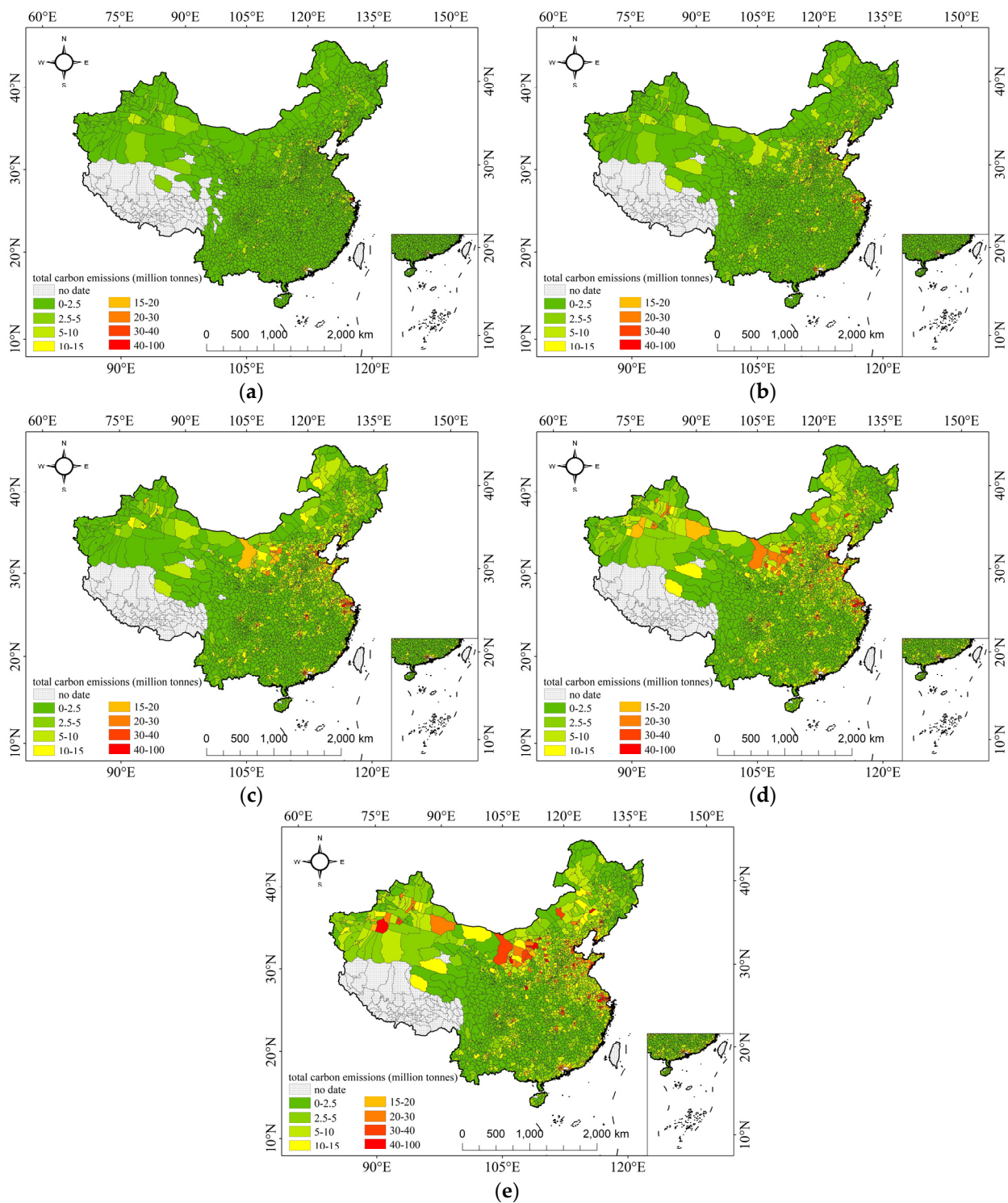**Figure 14.** County-scale carbon emissions (2000, 2005, 2010, 2015, 2019). (**a**) County-level carbon emissions in 2000. (**b**) County-level carbon emissions in 2005. (**c**) County-level carbon emissions in 2010. (**d**) County-level carbon emissions in 2015. (**e**) County-level carbon emissions in 2019.

In 2000, 98.45% of the counties in China had carbon emissions lower than 1×10^7 t. Six counties had carbon emissions greater than 2×10^7 t, and only Pudong New Area had carbon emissions greater than 3×10^7 t. In 2005, carbon emissions lower than 1×10^7 t

were observed in 93.98% of the counties. The number of counties with carbon emissions exceeding 2×10^7 t had risen to 25, while the number of counties with carbon emissions surpassing 3×10^7 t had increased to 7. In 2010, 87.85% of counties had carbon emissions less than 1×10^7 t, while the number of counties with carbon emissions greater than 2×10^7 t increased to 71, and the number of counties with carbon emissions greater than 3×10^7 t increased to 21. In 2015, 86.51% of counties had carbon emissions below 1×10^7 t, while the number of counties with emissions exceeding 2×10^7 t increased to 113, and the number of counties with emissions exceeding 3×10^7 t increased to 35. By contrast, in 2019, only 83.77% of counties had carbon emissions below the threshold of 1×10^7 t, while the number of counties with emissions greater than or equal to both thresholds rose significantly. There were 146 counties for the former and 61 for the latter.

The overall trend of county-level carbon emissions in China indicated a higher concentration in the eastern regions compared to the western regions, and a greater magnitude in the northern areas relative to the southern areas. In 2000, the number of high-carbon-emission areas at the county scale was low, and these areas had a dotted distribution. In 2005, high-carbon-emission areas increased, scattered in areas such as Beijing–Tianjin–Hebei, Shandong Peninsula, Jiangsu, Zhejiang, Shanghai, and the Pearl River Delta. In 2010, the number of high-carbon-emission areas increased rapidly, and these areas were characterized by a patchy distribution. The high values of carbon emissions were mainly concentrated in the following regions. (1) Tianjin, Shandong, Liaoning; (2) Shanghai; (3) Foshan, Zhongshan; (4) Ordos. Other high-value areas were sporadically located in the central and western parts of China. By 2015, high-carbon-emission areas continued to expand, especially the high-carbon-emission area in Ordos, which was centered around Alxa Left Banner, Etuoke Banner, and Dongsheng District. In 2019, urban areas such as Shaya County, Kuche County, Shihezi City, and Hami City in Xinjiang began to experience high carbon emissions, while the other major carbon emission centers significantly expanded. High-carbon-emission areas in the central and western regions still showed a dotted distribution, such as Banan District in Chongqing, Chenghua District in Chengdu, and Furong District in Changsha.

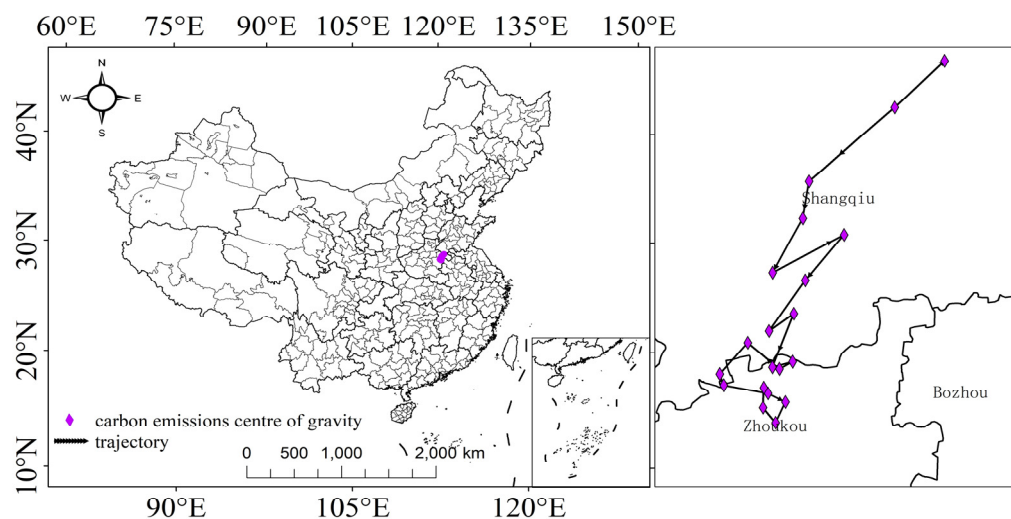*4.3. Analysis of the Spatial Dependence of China's Energy Carbon Emissions*

In this study, the CO_2 emission data from 2000 to 2019 were selected to calculate the centroid of China's CO_2 emissions, incorporating carbon emission weights corresponding to administrative boundaries as a means of capturing spatial variations in China's carbon emissions. Utilizing the center of gravity model, several key outcomes were obtained: the latitude and longitude coordinates of China's CO_2 emissions center of gravity from 2000 to 2019 (Table 5), the migration distance and rate of this center of gravity (Table 6), and the migration trajectory of this center of gravity (Figure 15).

Table 5. Latitude and longitude coordinates of the center of gravity of carbon emissions.

Year	2000	2001	2002	2003	2004
Longitude	115.74	115.63	115.44	115.43	115.35
Latitude	34.47	34.41	34.30	34.24	34.16
Year	2005	2006	2007	2008	2009
Longitude	115.50	115.41	115.33	115.38	115.33
Latitude	34.20	34.137	34.06	34.08	34.00
Year	2010	2011	2012	2013	2014
Longitude	115.37	115.34	115.29	115.23	115.23
Latitude	34.00	34.00	34.04	34.00	33.98
Year	2015	2016	2017	2018	2019
Longitude	115.31	115.34	115.32	115.30	115.31
Latitude	33.96	33.94	33.91	33.93	33.97

Table 6. Distance and rate of carbon emission transport.

Year	2000–2005	2005–2010	2010–2015	2015–2019
Distance (km)	37.00	25.29	7.23	1.29
Speed (km/y)	7.40	5.06	1.45	0.32

Figure 15. Carbon emission transport pathway in China.

As illustrated in Figure 15, the gravity center of carbon emission was located in Henan Province from 2000 to 2019. From 2000 to 2005, the gravity center of carbon emission shifted 37 km to the southwest, corresponding to 7.40 km/y. In the next 5 years, the same trend was observed but with a rate of 5.06 km/y. The move of this center further slowed down in 2010–2015 at a rate of 1.45 km/y to the southwest. However, this trend was slightly reversed from 2015 to 2019, with an average moving rate of 0.32 km/y to the northwest. The above analysis suggests that the gravity center of carbon emission shifted to the southwest, with a distance of 68.68 km, corresponding to 3.61 km/y.

4.4. Trend Analysis of Carbon Emissions in China

Figure 16 reflects the trend of carbon emissions growth at different scales in China from 2000 to 2019. The types of slow change (slow growth and slower growth) were more prevalent than rapid change (faster growth and rapid growth) and medium-speed change. Three provinces exhibited medium growth rates. The types of rapid changes were distributed in most parts of North China and the northern part of Central China. The type of slow change was distributed in the central and western regions and the northeast region. Among them, Shandong belonged to the category of rapid growth. Inner Mongolia and Jiangsu were faster-growing regions. Shanxi, Xinjiang, Hebei, and Guangdong were medium-growth models. The provinces exhibiting slower growth included Jilin, Liaoning, Yunnan, Guizhou, Sichuan, Hunan, Shaanxi, Zhejiang, and Fujian. Meanwhile, Heilongjiang, Hainan, Gansu, Qinghai, Beijing, and Tianjin were characterized by slow growth.

4.5. Projections of Energy Carbon Emissions

The forecast of China's carbon emissions based on the grey prediction model is depicted in Figure 17. In 2025, the average value of China's carbon emissions was 7.82×10^2 million tons. The provinces with emissions higher than the average value were Shandong (25.61×10^2 million tons), Jiangsu (16.39×10^2 million tons), Inner Mongolia (17.00×10^2 million tons), Hebei (15.54×10^2 million tons), Shanxi Province (14.16×10^2 million tons), Guangdong (12.70×10^2 million tons), Liaoning (11.54×10^2 million tons), Xinjiang (10.89×10^2 million tons), Henan (10.15×10^2 million tons), and Zhejiang (8.76×10^2 million tons). In 2030, the average value of China's carbon emissions was 9.44×10^2 million tons.

The provinces with emissions higher than the average value were Shandong (31.88×10^2 million tons), Jiangsu (20.10×10^2 million tons), Inner Mongolia (21.76×10^2 million tons), Hebei (18.50×10^2 million tons), Shanxi Province (16.77×10^2 million tons), Guangdong (15.22×10^2 million tons), Xinjiang (14.34×10^2 million tons), Liaoning (13.41×10^2 million tons), Henan (11.68×10^2 million tons), and Zhejiang (10.39×10^2 million tons). Spatial analysis indicates China's high-carbon-emission areas in 2025 and 2030 were mainly distributed in the northern part of the country.
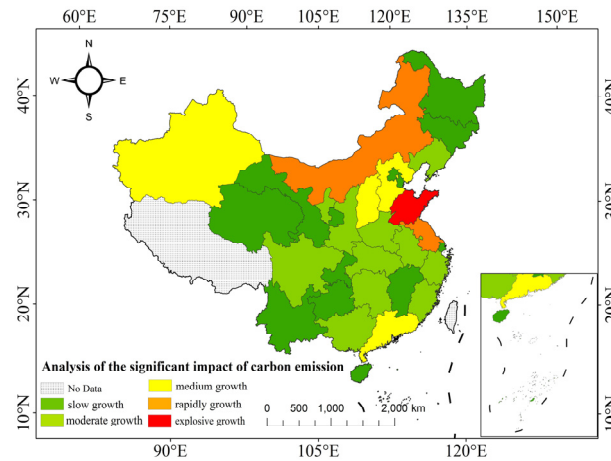

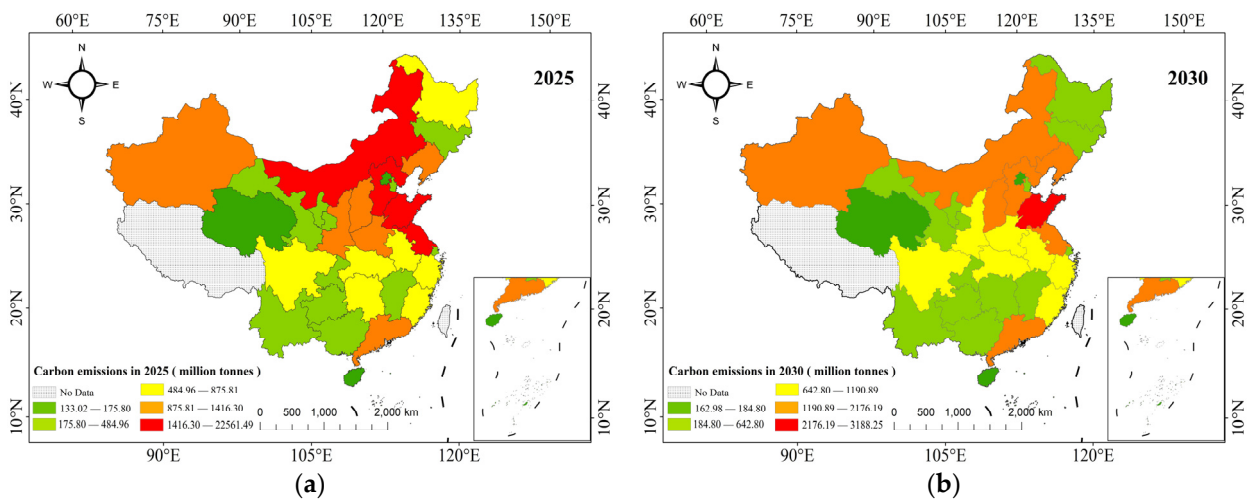**Figure 16.** Trend of carbon emissions in China.

Figure 17. Carbon emission projections (2025, 2030). (**a**) Carbon emission projections for 2025. (**b**) Carbon emission projections for 2030.

5. Discussion

With the rapid urbanization and economic development in China from 2000 to 2019, both national and provincial scales witnessed a continuous increase in total carbon emissions and per capita carbon emissions (Figures 3 and 4) [48]. However, advancements in science and technological innovation have led to improved energy utilization efficiency, resulting in a decline in the intensity of carbon emissions over time (Figure 5) [49]. To enhance our understanding of controlling total carbon emissions, this study investigated the relationship between carbon emissions and nighttime light brightness (Table 3). A model was constructed to assess carbon emissions at smaller scales (municipal and county levels) and analyze their spatial distribution characteristics (Figure 6).

China's carbon emissions displayed a discernible spatial pattern, characterized by higher levels in the northern regions compared to the southern regions and greater emission

levels in the eastern areas relative to the western ones [50]. Shandong Province, as a prominent industrial hub with highly carbon-intensive energy structures, ranked highest among all provinces for its substantial contribution to national carbon emissions (Figure 7) [51]. The center of gravity for China's overall carbon emissions was located within Henan Province, but had been shifting towards the southwest due to various factors (Figure 15). Those included the attraction of industries and population resulting in increased energy demand. Moreover, national policies aimed at addressing regional imbalances had facilitated industrial structure adjustments along with the relocation of traditional heavy industries towards the southwest region, further contributing to this phenomenon [52].

In this study, carbon emissions were calculated not only at the national and provincial levels but also at the municipal and county levels (Figures 13 and 14). This finding compensated for the lack of data at the city and county scales, thereby facilitating precise focus by national and local governments on achieving carbon emission control. The investigation of China's spatial distribution characteristics of carbon emissions holds significant importance in elucidating their spatial patterns and historical dynamics. In light of China's "dual carbon" goal, this research predicted that by 2025 and 2030 [53], the average carbon emissions would be 7.82×10^2 million tons and 9.44×10^2 million tons, respectively. These predictions provide valuable data support for formulating energy conservation and emission reduction policies in China.

As a prominent economic hub with a substantial population, Shandong has experienced a consistent rise in carbon emissions attributed to its robust economic development. The province's electric power industry is highly developed, particularly its coal-based sector which significantly contributes to its overall carbon emissions [54]. Located on the eastern coast of China, Shandong plays a crucial role as an industrial center encompassing 41 major industrial categories. Shandong exhibits both the highest current level of carbon emissions and the highest predicted future increases for two reasons (Figure 17): (1) The dominance of heavy industry in Shandong's economy will persist, leading to significant combustion of fossil fuels and consequent escalation in CO_2 emissions. (2) Plans are underway for major manufacturing industries such as automobile manufacturing and chemical materials within different industrial parks or bases, which will further contribute to elevated levels of carbon emissions.

The research still has some limitations, and the following issues need to be addressed: (1) The calculation of carbon emissions only considers energy consumption factors, neglecting carbon emission factors associated with construction, population, industry, and other aspects. (2) This research primarily focuses on carbon sources. However, it is crucial to consider the impact of carbon sinks on carbon emissions. Since the Industrial Revolution, there has been a substantial decline in forests and grasslands. Therefore, exploring monitoring methods for carbon sinks is imperative. (3) While this study accounts for carbon emissions at the city and county levels, further exploration is needed regarding accounting methods for smaller scales such as towns and villages as well as specific point sources of carbon emissions.

6. Conclusions

Utilizing nighttime light remote sensing, energy statistics, population spatial distribution, GDP spatial distribution, and other data, this study measured the total CO_2 emissions at national and provincial levels over the past 20 years using national statistics data. Nighttime-class EANTLI nighttime light data from 2000 to 2019 were utilized; the sum of DN values (T) was extracted; and the total CO_2 emissions and DN values were adopted to conduct a correlation analysis and linear, exponential, and logarithmic fitting. The best function was selected for conversion model construction. The provincial conversion model was improved; the total CO_2 emissions at municipal and county levels where data are missing were measured; and the characteristics of China's carbon emissions (total carbon emissions, per capita carbon emissions, and carbon emission intensity), spatial scale of carbon emissions (national, provincial, municipal, and county scales), and spatial pattern

of carbon emissions (center of gravity migration and trend analysis) were analyzed. Then, the carbon emissions in China were forecasted. The conclusions are as follows:

(1) Nationally, from 2000 to 2019, the total amount of carbon emissions generally increased annually. The total amount rose from 4.42 Gt to 15.83 Gt, with an average annual growth rate of 7.08%. Per capita carbon emissions showed an increasing trend, rising from 3.49 t/person to 11.23 t/person, with an average annual growth rate of 6.48%. The overall trend of China's carbon emission intensity during 2000~2019 displayed a decreasing trend, decreasing from 4.41 tons per CNY 1 million to 1.60 tons per CNY 1 million, with an average annual decrease of 5.09%.

(2) The fitting comparison indicated that the correlation coefficients of the exponential, linear, and logarithmic models were high, with their mean R^2 value exceeding 0.7. The logarithmic model exhibited the best fitting effect, with a mean R^2 value of 0.83. Therefore, a logarithmic model was chosen for the conversion calculation of energy carbon emissions and the sum of DN values.

(3) The center of gravity of carbon emissions was located within Henan Province in China, with a general tendency to move from west to south. The migration of the center of gravity of carbon emissions indicated an increasing proportion and higher growth rate of carbon emissions in the western and southern regions compared to other parts of the country.

(4) Based on the grey prediction model GM (1, 1), China's carbon emissions for 2025 and 2030 were predicted. In 2025, the average value of China's carbon emissions is predicted to be 7.82×10^2 million tons, with Shandong Province having the highest emissions at 225.61×10^2 million tons. In 2030, the average value is expected to be 9.44×10^2 million tons, with Shandong Province remaining the highest at 31.88×10^2 million tons.

As a result of an analysis of the spatial scale of carbon emissions, a carbon emission accounting model was constructed, which solved the problem of a large amount of missing statistical data at the city and county levels during carbon emission accounting. By using nighttime light data to measure carbon emissions, a more detailed scale of carbon emissions could be obtained. This achieved the clarity and targeting of China's total carbon emission control goals. To better achieve the goal of carbon neutrality, China needs to emphasize the need to comprehensively consider the impact of different environments, industrial structures, and socio-economic characteristics during formulation. The results of this study offer valuable insights for the scientific development of China's low-carbon economy and the strategic formulation of carbon emission policies.

Author Contributions: Conceptualization, Z.Z. and Y.S.; methodology, Z.Z. and S.F.; validation, Z.Z. and J.L.; formal analysis, Z.S.; investigation, Y.S., S.F. and J.L.; data curation, S.F., J.L. and Y.Q.; writing—original draft preparation, Z.Z. and Y.S.; writing—review and editing, Z.Z.; funding acquisition, Y.S. All authors have read and agreed to the published version of the manuscript.

Data Availability Statement: The nighttime light remote sensing data are available from https://www.geodoi.ac.cn/WebCn/doi.aspx?Id=3100, accessed on 1 January 2023. The statistical data can be obtained from https://data.stats.gov.cn/, accessed on 1 May 2020.

Conflicts of Interest: The authors declare no conflict of interest.

References

1. Radočaj, D.; Obhođaš, J.; Jurišić, M.; Gašparović, M. Global Open Data Remote Sensing Satellite Missions for Land Monitoring and Conservation: A Review. *Land* **2020**, *9*, 402. [CrossRef]
2. Shiklomanov, A.N.; Bradley, B.A.; Dahlin, K.M.; Fox, A.M.; Gough, C.M.; Hoffman, F.M.; Middleton, E.M.; Serbin, S.P.; Smallman, L.; Smith, W.K. Enhancing Global Change Experiments through Integration of Remote-Sensing Techniques. *Front. Ecol. Environ.* **2019**, *17*, 215–224. [CrossRef]

3. Zhang, H.; Huang, M.; Qing, X.; Li, G.; Tian, C. Bibliometric Analysis of Global Remote Sensing Research during 2010–2015. *ISPRS Int. J. Geo-Inf.* **2017**, *6*, 332. [CrossRef]

4. Akbari, E.; Alavipanah, S.K.; Jeihouni, M.; Hajeb, M.; Haase, D.; Alavipanah, S. A Review of Ocean/Sea Subsurface Water Temperature Studies from Remote Sensing and Non-Remote Sensing Methods. *Water* **2017**, *9*, 936. [CrossRef]

5. Roy, I. Addressing on Abrupt Global Warming, Warming Trend Slowdown and Related Features in Recent Decades. *Front. Earth Sci.* **2018**, *6*, 136. [CrossRef]

6. Fang, J.; Zhu, J.; Wang, S.; Yue, C.; Shen, H. Global Warming, Human-Induced Carbon Emissions, and Their Uncertainties. *Sci. China Earth Sci.* **2011**, *54*, 1458–1468. [CrossRef]

7. Lenton, T.M.; Xu, C.; Abrams, J.F.; Ghadiali, A.; Loriani, S.; Sakschewski, B.; Zimm, C.; Ebi, K.L.; Dunn, R.R.; Svenning, J.-C.; et al. Quantifying the Human Cost of Global Warming. *Nat. Sustain.* **2023**, *6*, 1237–1247. [CrossRef]

8. Yoro, K.O.; Daramola, M.O. CO_2 Emission Sources, Greenhouse Gases, and the Global Warming Effect. In *Advances in Carbon Capture*; Elsevier: Amsterdam, The Netherlands, 2020; pp. 3–28.

9. Zhang, T.; Zhang, W.; Yang, R.; Liu, Y.; Jafari, M. CO_2 Capture and Storage Monitoring Based on Remote Sensing Techniques: A Review. *J. Clean. Prod.* **2021**, *281*, 124409. [CrossRef]

10. Jeffry, L.; Ong, M.Y.; Nomanbhay, S.; Mofijur, M.; Mubashir, M.; Show, P.L. Greenhouse Gases Utilization: A Review. *Fuel* **2021**, *301*, 121017. [CrossRef]

11. Mikhaylov, A.; Moiseev, N.; Aleshin, K.; Burkhardt, T. Global Climate Change and Greenhouse Effect. *Entrep. Sustain. Issues* **2020**, *7*, 2897. [CrossRef]

12. Lee, H.; Calvin, K.; Dasgupta, D.; Krinner, G.; Mukherji, A.; Thorne, P.; Trisos, C.; Romero, J.; Aldunce, P.; Barrett, K.; et al. *AR6 Synthesis Report: Climate Change 2023*; Summary for Policymakers; United Nations Intergovernmental Panel on Climate Change: Interlaken, Switzerland, 2023.

13. Chen, J.; Gao, M.; Huang, S.; Hou, W. Application of Remote Sensing Satellite Data for Carbon Emissions Reduction. *J. Chin. Econ. Bus. Stud.* **2021**, *19*, 109–117. [CrossRef]

14. Shang, M.; Ma, Z.; Su, Y.; Shaheen, F.; Khan, R.; Mohd Tahir, L.; Khalid Anser, M.; Zaman, K. Understanding the Importance of Sustainable Ecological Innovation in Reducing Carbon Emissions: Investigating the Green Energy Demand, Financial Development, Natural Resource Management, Industrialisation and Urbanisation Channels. *Econ. Res.* **2023**, *36*, 2137823. [CrossRef]

15. Gregg, J.S.; Andres, R.J.; Marland, G. China: Emissions Pattern of the World Leader in CO_2 Emissions from Fossil Fuel Consumption and Cement Production. *Geophys. Res. Lett.* **2008**, *35*, 1–5. [CrossRef]

16. Zhang, X.; Geng, Y.; Shao, S.; Wilson, J.; Song, X.; You, W. China's Non-Fossil Energy Development and Its 2030 CO_2 Reduction Targets: The Role of Urbanization. *Appl. Energy* **2020**, *261*, 114353. [CrossRef]

17. Zheng, J.; Mi, Z.; Coffman, D.; Milcheva, S.; Shan, Y.; Guan, D.; Wang, S. Regional Development and Carbon Emissions in China. *Energy Econ.* **2019**, *81*, 25–36. [CrossRef]

18. Wang, Y.; Guo, C.; Chen, X.; Jia, L.; Guo, X.; Chen, R.; Zhang, M.; Chen, Z.; Wang, H. Carbon Peak and Carbon Neutrality in China: Goals, Implementation Path and Prospects. *China Geol.* **2021**, *4*, 720–746. [CrossRef]

19. Obland, M.D.; Campbell, J.; Kooi, S.; Fan, T.F.; Carrion, W.; Hicks, J.; Lin, B.; Nehrir, A.R.; Browell, E.V.; Meadows, B.; et al. Technology Advancements for Active Remote Sensing of Carbon Dioxide from Space Using the Active Sensing of CO_2 Emissions over Nights, Days, and Seasons (ASCENDS) CarbonHawk Experiment Simulator. *EPJ Web Conf.* **2018**, *176*, 02018. [CrossRef]

20. Scheibenreif, L.M.; Mommert, M.; Borth, D. Estimation of Air Pollution with Remote Sensing Data: Revealing Greenhouse Gas Emissions from Space. *arXiv* **2021**, arXiv:2108.13902.

21. Penman, J.; Baltuck, M.; Green, C.; Olofsson, P.; Raison, J.; Woodcock, C. *Integrating Remote-Sensing and Ground-Based Observations for Estimation of Emissions and Removals of Greenhouse Gases in Forests: Methods and Guidance from Global Forest Observation Initiative*; GEO-GFOI MGD Document Version 1.0; Global Forest Observations Initiative: Geo Geneva, Switzerland, 2014.

22. Xiu, L.; Ling-Xue, W.; Wei-Qi, J.; Xia, W. The Development of Optical Remote Measurement for Hazardous Gas Leakage. *Infrared Technol.* **2009**, *31*, 562–563.

23. Global Forest Observations Initiative. *Integration of Remote-Sensing and Ground-Based Observations for Estimation of Emissions and Removals of Greenhouse Gases in Forests: Methods and Guidance from the Global Forest Observations Initiative*; Edition 2.0; Global Forest Observations Initiative: Geneva, Switzerland, 2016.

24. Ju, T.; Liang, Z.; Liu, W.; Li, B.; Huang, R.; Geng, T. Monitoring of Air Pollution by Remote Sensing in Lanzhou City from 2010 to 2019. *Water Air Soil Pollut.* **2022**, *233*, 359. [CrossRef]

25. Tanaka, K.; Hayami, H.; Saino, H.; Miura, K.; Itahashi, S.; Saito, S. Three-Dimensional Analysis of Haze by PM2.5 and Other Pollutants Based on Ground- and Elevated-Level Monitoring in Central Tokyo: Example in Early Part of December 2015. *J. Jpn. Soc. Atmos. Environ.* **2017**, *52*, 51–58.

26. Liu, Z.; Sun, Y.; Zeng, Y.; Guan, Y.; Huang, Y.; Chen, Y.; Li, D.; Mo, L.; Chen, S.; Mai, B. Semi-Volatile Organic Compounds in Fine Particulate Matter on a Tropical Island in the South China Sea. *J. Hazard. Mater.* **2022**, *426*, 128071. [CrossRef]

27. Gao, F.; Wu, J.; Xiao, J.; Li, X.; Liao, S.; Chen, W. Spatially Explicit Carbon Emissions by Remote Sensing and Social Sensing. *Environ. Res.* **2023**, *221*, 115257. [CrossRef]

28. Zhao, M.; Zhou, Y.; Li, X.; Cao, W.; He, C.; Yu, B.; Li, X.; Elvidge, C.D.; Cheng, W.; Zhou, C. Applications of Satellite Remote Sensing of Nighttime Light Observations: Advances, Challenges, and Perspectives. *Remote Sens.* **2019**, *11*, 1971. [CrossRef]

29. Liu, Z. Near-Real-Time Methodology for Assessing Global Carbon Emissions. *Chin. Sci. Bull. Chin.* **2023**, *68*, 830–840. [CrossRef]

30. De Sy, V.; Herold, M.; Achard, F.; Avitabile, V.; Baccini, A.; Carter, S.; Clevers, J.G.; Lindquist, E.; Pereira, M.; Verchot, L. Tropical Deforestation Drivers and Associated Carbon Emission Factors Derived from Remote Sensing Data. *Environ. Res. Lett.* **2019**, *14*, 094022. [CrossRef]

31. Pohl, C.; Van Genderen, J.L. Review Article Multisensor Image Fusion in Remote Sensing: Concepts, Methods and Applications. *Int. J. Remote Sens.* **1998**, *19*, 823–854. [CrossRef]

32. Zhang, Z.; Xu, W.; Qin, Q.; Long, Z. Downscaling Solar-Induced Chlorophyll Fluorescence Based on Convolutional Neural Network Method to Monitor Agricultural Drought. *IEEE Trans. Geosci. Remote Sens.* **2020**, *59*, 1012–1028. [CrossRef]

33. Shanmugapriya, P.; Rathika, S.; Ramesh, T.; Janaki, P. Applications of Remote Sensing in Agriculture-A Review. *Int. J. Curr. Microbiol. Appl. Sci* **2019**, *8*, 2270–2283. [CrossRef]

34. Zhang, Z.; Xu, W.; Shi, Z.; Qin, Q. Establishment of a Comprehensive Drought Monitoring Index Based on Multisource Remote Sensing Data and Agricultural Drought Monitoring. *IEEE J. Sel. Top. Appl. Earth Obs. Remote Sens.* **2021**, *14*, 2113–2126. [CrossRef]

35. Chen, C.; Liang, J.; Xie, F.; Hu, Z.; Sun, W.; Yang, G.; Yu, J.; Chen, L.; Wang, L.; Wang, L.; et al. Temporal and Spatial Variation of Coastline Using Remote Sensing Images for Zhoushan Archipelago, China. *Int. J. Appl. Earth Obs. Geoinf.* **2022**, *107*, 102711. [CrossRef]

36. Chen, C.; Liang, J.; Yang, G.; Sun, W. Spatio-Temporal Distribution of Harmful Algal Blooms and Their Correlations with Marine Hydrological Elements in Offshore Areas, China. *Ocean Coast. Manag.* **2023**, *238*, 106554. [CrossRef]

37. Wu, H.; Li, Z.-L. Scale Issues in Remote Sensing: A Review on Analysis, Processing and Modeling. *Sensors* **2009**, *9*, 1768–1793. [CrossRef]

38. Zhang, L.; Zhang, J.; Li, X.; Zhou, K.; Ye, J. The Impact of Urban Sprawl on Carbon Emissions from the Perspective of Nighttime Light Remote Sensing: A Case Study in Eastern China. *Sustainability* **2023**, *15*, 11940. [CrossRef]

39. Chen, J.; Gao, M.; Cheng, S.; Liu, X.; Hou, W.; Song, M.; Li, D.; Fan, W. China's City-Level Carbon Emissions during 1992–2017 Based on the Inter-Calibration of Nighttime Light Data. *Sci. Rep.* **2021**, *11*, 3323. [CrossRef]

40. Gu, C. Urbanization: Processes and Driving Forces. *Sci. China Earth Sci.* **2019**, *62*, 1351–1360. [CrossRef]

41. Zhou, Y.; Wang, H.; Qiu, H. Population Aging Reduces Carbon Emissions: Evidence from China's Latest Three Censuses. *Appl. Energy* **2023**, *351*, 121799. [CrossRef]

42. Zhong, X.; Yan, Q.; Li, G. Long Time Series Nighttime Light Dataset of China (2000–2020). *Digit. J. Glob. Chang. Data Repos* **2022**, *6*, 416–424.

43. Shan, Y.; Guan, D.; Liu, J.; Mi, Z.; Liu, Z.; Liu, J.; Schroeder, H.; Cai, B.; Chen, Y.; Shao, S.; et al. Methodology and Applications of City Level CO_2 Emission Accounts in China. *J. Clean. Prod.* **2017**, *161*, 1215–1225. [CrossRef]

44. Shi, K.; Chen, Y.; Yu, B.; Xu, T.; Chen, Z.; Liu, R.; Li, L.; Wu, J. Modeling Spatiotemporal CO_2 (Carbon Dioxide) Emission Dynamics in China from DMSP-OLS Nighttime Stable Light Data Using Panel Data Analysis. *Appl. Energy* **2016**, *168*, 523–533. [CrossRef]

45. Zhang, Z.; Xu, W.; Qin, Q.; Chen, Y. Monitoring and Assessment of Agricultural Drought Based on Solar-Induced Chlorophyll Fluorescence during Growing Season in North China Plain. *IEEE J. Sel. Top. Appl. Earth Obs. Remote Sens.* **2020**, *14*, 775–790. [CrossRef]

46. Wang, Y.; Xia, T.; Shataer, R.; Zhang, S.; Li, Z. Analysis of Characteristics and Driving Factors of Land-Use Changes in the Tarim River Basin from 1990 to 2018. *Sustainability* **2021**, *13*, 10263. [CrossRef]

47. Wang, Y.; Dang, Y.; Li, Y.; Liu, S. An Approach to Increase Prediction Precision of GM (1, 1) Model Based on Optimization of the Initial Condition. *Expert Syst. Appl.* **2010**, *37*, 5640–5644. [CrossRef]

48. Yang, T.; Liu, J.; Mi, H.; Cao, Z.; Wang, Y.; Han, H.; Luan, J.; Wang, Z. An Estimating Method for Carbon Emissions of China Based on Nighttime Lights Remote Sensing Satellite Images. *Sustainability* **2022**, *14*, 2269. [CrossRef]

49. Guan, D.; Meng, J.; Reiner, D.M.; Zhang, N.; Shan, Y.; Mi, Z.; Shao, S.; Liu, Z.; Zhang, Q.; Davis, S.J. Structural Decline in China's CO_2 Emissions through Transitions in Industry and Energy Systems. *Nat. Geosci.* **2018**, *11*, 551–555. [CrossRef]

50. Cai, B.; Wang, X.; Huang, G.; Wang, J.; Cao, D.; Baetz, B.W.; Liu, L.; Zhang, H.; Fenech, A.; Liu, Z. Spatiotemporal Changes of China's Carbon Emissions. *Geophys. Res. Lett.* **2018**, *45*, 8536–8546. [CrossRef]

51. Zhu, L.; Xing, H.; Hou, D. Analysis of Carbon Emissions from Land Cover Change during 2000 to 2020 in Shandong Province, China. *Sci. Rep.* **2022**, *12*, 8021. [CrossRef]

52. Xiao, D.; Niu, H.; Guo, J.; Zhao, S.; Fan, L. Carbon Storage Change Analysis and Emission Reduction Suggestions under Land Use Transition: A Case Study of Henan Province, China. *Int. J. Environ. Res. Public Health* **2021**, *18*, 1844. [CrossRef]

53. Wen, L.; Diao, P. Simulation Study on Carbon Emission of China's Electricity Supply and Demand under the Dual-Carbon Target. *J. Clean. Prod.* **2022**, *379*, 134654. [CrossRef]

54. Liu, K.; Wang, J.; Kang, X.; Liu, J.; Xia, Z.; Du, K.; Zhu, X. Spatio-Temporal Analysis of Population-Land-Economic Urbanization and Its Impact on Urban Carbon Emissions in Shandong Province, China. *Land* **2022**, *11*, 266. [CrossRef]